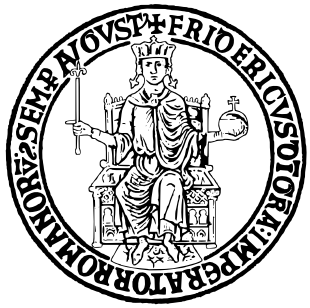


UNIVERSITÀ DEGLI STUDI DI NAPOLI FEDERICO II



SCUOLA POLITECNICA E DELLE SCIENZE DI BASE

INGEGNERIA DELL'AUTOMAZIONE E ROBOTICA

NONLINEAR DYNAMICS AND CONTROL

ANALYSIS AND CONTROL OF THE CIMA REACTION

Prof. Mario DI BERNARDO

Giulia Gelsomina ROMANO
P38000223

March 2025

Contents

Introduction	2
1 Chlorine Dioxide–Iodine–Malonic Acid Model	3
1.1 CIMA Reaction	3
2 Open Loop Analysis	6
2.1 Equilibrium Point	6
2.2 Phase Plane Analysis	8
2.3 Bifurcation Analysis	12
3 Control Synthesis	15
3.1 Linear LQ Optimal Control	16
3.2 I/O Feedback Linearization	23
3.3 Sliding Mode Control	30
4 Robustness Analysis	38
4.1 Disturbance on the Input	38
4.2 Parametric Uncertainties	43
5 Conclusion and Controllers Comparison	48
Bibliography	51

Introduction

In this study, an open-loop analysis and a control synthesis are applied to the Chlorine Dioxide–Iodine–Malonic Acid (CIMA) reaction [1, 2]. This project is structured into the following main chapters:

- **Chapter 1** introduces the chemical reactions and revises the nonlinear model. It explains the state variables and the parameters that characterize the system.
- **Chapter 2** focuses on the Open Loop Analysis. Specifically, using Pplane [4], system trajectories are analyzed by varying one of the key model parameters. Additionally, a bifurcation analysis is conducted using MatCont [5].
- **Chapter 3** presents the synthesis of the control problem, aiming to regulate the reaction through a control input with specific desired performances. Three controllers are implemented: the Linear Quadratic (LQ) Optimal Controller, designed using the linearized model around an equilibrium point of interest, and two nonlinear control techniques the Feedback Linearization (FBL) Controller and the Sliding Mode (SM) Controller. The controllers are tested using both a constant reference and a sinusoidal reference.
- **Chapter 4** focuses on the robustness analysis of the three controllers, evaluating their performance in presence of input disturbance and parametric uncertainties.

Finally, the project concludes with a summary of the simulation results, providing a comparative analysis of the controllers' performance.

ChatGPT has been occasionally used for text revision and to check the accuracy of translations.

Chapter 1

Chlorine Dioxide–Iodine–Malonic Acid Model

1.1 CIMA Reaction

In the early 1950s, the Russian biochemist Boris Belousov, while studying the metabolic processes that occur in living cells, observed that his chemical reaction spontaneously oscillated dozens of times before finally reaching equilibrium. His research was not taken seriously, and it was only ten years later that the graduate student Zhabotinsky investigated the reaction sequence in detail. The Belousov-Zhabotinsky (BZ) reaction, as it came to be known, became a pioneering discovery in the field of oscillating chemical reactions [1].

In a similar spirit, in 1990, Lengyel et al. proposed and analyzed a particularly elegant model of another oscillating reaction, the chlorine dioxide-iodine-malonic acid ($ClO_2 - I_2 - MA$) [1]. This reaction mixture contains chlorine dioxide (ClO_2), iodine (I_2) and malonic acid (MA). Lengyel's group demonstrated how these components interact and evolve within the system. They considered the following three component reactions and their empirical rate laws.

N.	Reaction	Empirical Rate Law
1	$MA + I_2 \rightarrow IMA + I^- + H^+$	$\frac{d[I_2]}{d\tau} = -\frac{k_{1a}[MA][I_2]}{k_{1b}+[I_2]}$
2	$ClO_2 + I^- \rightarrow ClO_2^- + \frac{1}{2}I_2$	$\frac{d[ClO_2]}{d\tau} = -k_2[ClO_2][I^-]$
3	$ClO_2 + 4I^- + 4H^+ \rightarrow Cl^- + 2I_2 + 2H_2O$	$\frac{d[ClO_2^-]}{d\tau} = -k_{3a}[ClO_2^-][I^-][H^+] - k_{3b}[ClO_2^-][I_2]\frac{[I^-]}{k_u+[I^-]^2}$

Table 1.1: CIMA Reactions and Empirical Rate Laws

In Table 1.1, the following reactions take place [2]:

1. The iodination of malonic acid MA as a continuous source of iodide I^- ;
2. The oxidation of iodide ions I^- by free chlorine dioxide ClO_2 providing chlorite ions ClO_2^- ;

3. The reaction between the iodide I^- formed in Reaction 1 and the chlorite ions ClO_2^- produced in Reaction 2.

The reaction rate constants used are $k_{1a} = 7.5 \times 10^{-3} M^{-1}s^{-1}$, $k_2 = 6.0 \times 10^3 M^{-1}s^{-1}$, $k_{3a} = 4.6 \times 10^2 M^{-2}s^{-1}$, $k_{3b} = 2.65 \times 10^{-3}s^{-1}$, whereas $k_{1b} = 5 \times 10^{-5}M$ at $Ph2$, $k_u = 1.0 \times 10^{-14}M^2$ describe saturation phenomena [3].

During their simulations, they found out that the reactants MA , I_2 , and ClO_2 vary much more slowly than the intermediates I^- and ClO_2^- . Thanks to this discovery, by approximating the concentrations of the slow reactants as constants and making other reasonable simplifications, they were able to reduce the complex system to a two-variable model [1].

By scaling properly the rate constants:

$$k'_1 = k_{1a}[MA]_0, \quad k'_2 = k_2[ClO_2], \quad k'_3 = k_{3b}[I_2]_0 \quad (1.1)$$

the resulting simplified reaction system is:

N.	Reaction	Empirical Rate Law
1	$I_2 \rightarrow I^-$	$\frac{d[I_2]}{d\tau} = k'_1$
2	$I^- \rightarrow ClO_2^-$	$\frac{d[I^-]}{d\tau} = k'_2[I^-]$
3	$4I^- + ClO_2^- \rightarrow P$	$\frac{d[ClO_2^-]}{d\tau} = \frac{k'_3[I^-][ClO_2^-]}{(k_u + [I^-]^2)}$

Table 1.2: Simplified CIMA Reactions and Empirical Rate Laws

The Law of Mass Action is applied to the chemical reactions in Table 1.2 to obtain the following dynamical system:

$$\frac{d[I^-]}{d\tau} = k'_1 - k'_2[I^-] - 4 \frac{k'_3[I^-][ClO_2^-]}{(k_u + [I^-]^2)} \quad (1.2a)$$

$$\frac{d[ClO_2^-]}{d\tau} = k'_2[I^-] - \frac{k'_3[I^-][ClO_2^-]}{(k_u + [I^-]^2)} \quad (1.2b)$$

To further simplify the system, the iodide (I^-) concentration and chlorite (ClO_2^-) concentration are defined respectively as:

$$X = [I^-], \quad Y = [ClO_2^-] \quad (1.3)$$

and the variables and constants are scaled as in (1.4)

$$X = \alpha x, \quad Y = \beta y, \quad \tau = t\gamma, \quad \alpha = k_u^{1/2}, \quad (1.4)$$

$$\beta = \frac{k_u k'_2}{k'_3}, \quad \gamma = \frac{1}{k'_2}, \quad a = k'_1 \frac{\gamma}{\alpha}, \quad b = \frac{\alpha}{\beta}$$

where

- x and y are the dimensionless concentration of (I^-) and concentration of (ClO_2^-), respectively;

- α and β are the scaling factors based on the system parameters;
- $a > 0$ and $b > 0$ represent kinetic parameters.

Just for clarity in control applications, the state variables are renamed as:

$$x_1 = x, \quad x_2 = y \quad (1.5)$$

In this way, it is possible to put the resulting system of differential equations into dimensionless form (1.6a) and (1.6b).

$$\dot{x}_1 = a - x_1 - \frac{4x_1x_2}{1 + x_1^2} \quad (1.6a)$$

$$\dot{x}_2 = b \left(x_1 - \frac{x_1x_2}{1 + x_1^2} \right) \quad (1.6b)$$

This is a second order nonlinear system, characterized by a product term between x_1 and x_2 and by the term x_1^2 at the denominator.

Since x_1 and x_2 are chemical concentrations, they are positive ($x_1, x_2 \geq 0$). The system is influenced by the parameters a and b , defined as before. In particular, a has been set to 10 and, to identify possible codimension 1 bifurcations, the parameter b is varied within an interval of interest.

Chapter 2

Open Loop Analysis

2.1 Equilibrium Point

First of all, the equilibria of the system must be identified. To find the equilibrium points, the vector field of the system given by (1.6a) and (1.6b) is set to zero:

$$0 = a - \bar{x}_1 - \frac{4\bar{x}_1\bar{x}_2}{1 + \bar{x}_1^2} \quad (2.1a)$$

$$0 = b \left(\bar{x}_1 - \frac{\bar{x}_1\bar{x}_2}{1 + \bar{x}_1^2} \right) \quad (2.1b)$$

Solving algebraically (2.1a) and (2.1b), it is possible to determine the steady state solution $\bar{x} = (\bar{x}_1, \bar{x}_2)$.

In particular, this system has only one equilibrium point:

$$\bar{x} = \begin{bmatrix} \frac{a}{5} \\ 1 + \frac{a^2}{25} \end{bmatrix} \quad (2.2)$$

Now it is important to study the stability of the equilibrium point (2.2). For this porpoise, the Jacobian is computed:

$$J = \frac{\partial f(x)}{\partial x} = \begin{bmatrix} \frac{8x_1^2 x_2}{(1+x_1^2)^2} - \frac{4x_2}{(1+x_1^2)} - 1 & -\frac{4x_1}{(1+x_1^2)} \\ \frac{2bx_1^2 x_2}{(1+x_1^2)^2} - b \left(\frac{x_2}{(1+x_1^2)} - 1 \right) & -\frac{bx_1}{(1+x_1^2)} \end{bmatrix} \quad (2.3)$$

Evaluating the Jacobian matrix at the equilibrium point (\bar{x}_1, \bar{x}_2) and considering that $\bar{x}_2 = (1 + \bar{x}_1^2)$:

$$J(\bar{x}_1, \bar{x}_2) = \begin{bmatrix} \frac{8\bar{x}_1^2}{(1+\bar{x}_1^2)} - 5 & -\frac{4\bar{x}_1}{(1+\bar{x}_1^2)} \\ \frac{2b\bar{x}_1^2}{(1+\bar{x}_1^2)} & -\frac{b\bar{x}_1}{(1+\bar{x}_1^2)} \end{bmatrix} = \frac{1}{(1 + \bar{x}_1^2)} \begin{bmatrix} 3\bar{x}_1^2 - 5 & -4\bar{x}_1 \\ 2b\bar{x}_1^2 & -b\bar{x}_1 \end{bmatrix} \quad (2.4)$$

The Jacobian evaluated in \bar{x} strictly depends on the parameter b and, since \bar{x}_1 is a function of a , it also depends on the parameter a .

Now considering $a = 10$, the equilibrium point is

$$\bar{x} = \begin{bmatrix} 2 \\ 5 \end{bmatrix} \quad (2.5)$$

Computing the determinant and the trace of $J(\bar{x})$ [1]:

$$\Delta(J(\bar{x})) = \frac{5b\bar{x}_1}{1 + \bar{x}_1^2} = 2b \quad (2.6)$$

$$\tau(J(\bar{x})) = \frac{3\bar{x}_1^2 - 5 - b\bar{x}_1}{1 + \bar{x}_1^2} = \frac{7 - 2b}{5} \quad (2.7)$$

Since b is positive by definition, the determinant $\Delta(J(\bar{x}))$ is always positive, as shown in Fig. 2.1. This confirms that the equilibrium point is never a saddle point.

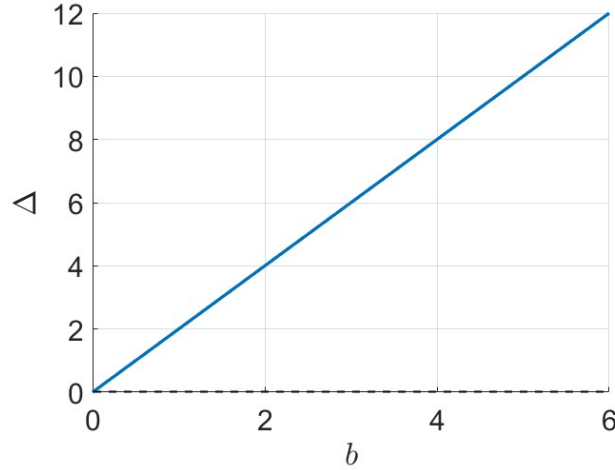


Figure 2.1: Determinant of J evaluated at the equilibrium point \bar{x} varying the parameter b .

Now it's time to compute $\tau^2 - 4\Delta$:

$$\tau(J(\bar{x}))^2 - 4\Delta(J(\bar{x})) = \frac{13^2 + 4b^2 - 52b}{25} - 8b = \frac{4b^2 - 252b + 169}{25} \quad (2.8)$$

As shown in Fig. 2.2, $\tau^2 - 4\Delta$ is positive until $b_{c1} \approx 0.216$ where the equilibrium point is a node. Beyond this point, the equilibrium becomes a spiral.

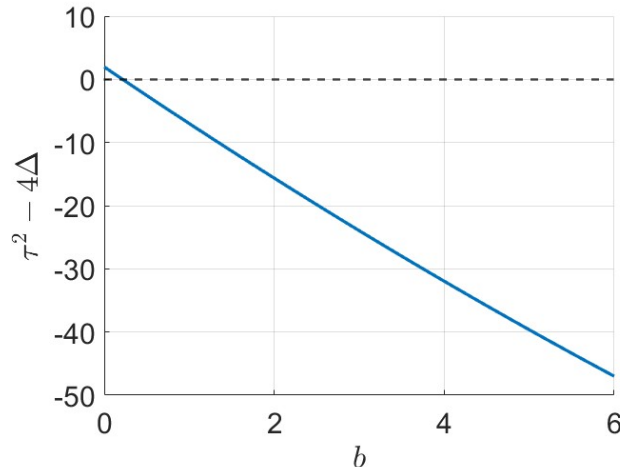


Figure 2.2: $\tau(J(\bar{x}))^2 - 4\Delta(J(\bar{x}))$ varying the parameter b . The transition from a node to a spiral occurs at $b = 0.216$.

As far as the sign of τ is concerned, it depends on:

$$\tau(J(\bar{x})) = 0 \rightarrow b_{c2} = 3.5 \quad (2.9)$$

So τ is positive for $b < b_{c2} = 3.5$ meaning that the equilibrium point is unstable. And for $b > b_{c2} = 3.5$, τ becomes negative, meaning that the equilibrium point is stable, as shown in Fig. 2.3. This suggests that a bifurcation may occur at $b_{c2} = 3.5$.

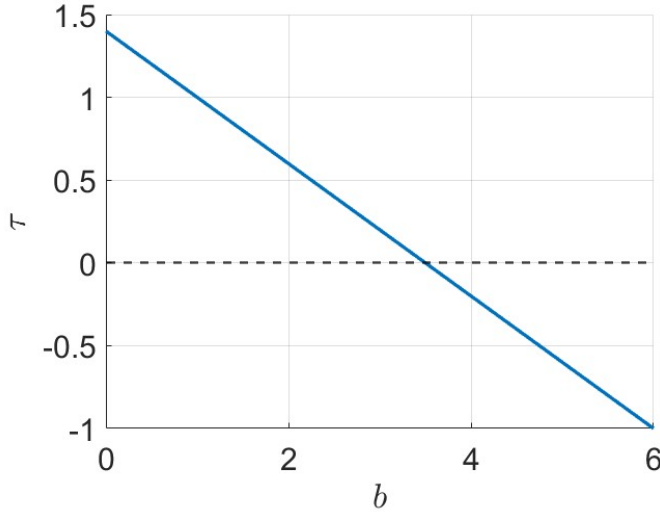


Figure 2.3: Trace of J evaluated at the equilibrium point \bar{x} varying the parameter b . The stability transition occurs at $b = b_{c2} = 3.5$.

2.2 Phase Plane Analysis

To prove the previous statements, the phase portrait of the system is plotted using the software PPlane [4].

Since the equilibrium point, as defined in (2.2), depends only on the parameter a , which is fixed, it's already known that its position $\bar{x} = (2, 5)^T$ will not change. However, as already analyzed, the type of equilibrium and its stability will vary depending on the parameter b . In order to verify it, based on the previous analysis, three different values of b are considered:

1. $b = 0.1$, where the equilibrium \bar{x} is expected to be an unstable node;
2. $b = 2$, where the equilibrium \bar{x} is expected to be an unstable spiral;
3. $b = 5$, where the equilibrium \bar{x} is expected to be a stable spiral.

Case 1: $b = 0.1$

As shown in Fig. 2.4, the position of the equilibrium point is confirmed at $\bar{x} = (2, 5)^T$. As far as the classification is concerned, it is a node. Additionally, the eigenvalues are real and both positive, indicating that the equilibrium point is unstable. The trajectories initially goes away from the equilibrium point $\bar{x} = (2, 5)^T$, then they are attracted to a stable limit cycle, in accordance with the Poincarè-Bendixson theorem [1] since the chemicals' concentrations are bounded [2]. This is visible in the phase portrait in Fig. 2.5.

Equilibrium Point:

There is a nodal source at $(2, 5)$

Jacobian:

$$\begin{array}{cc} 1.4 & -1.6 \\ 0.16 & -0.04 \end{array}$$

The eigenvalues and eigenvectors are:

$$1.1922 \quad (0.99168, 0.12876)$$

$$0.16775 \quad (0.79227, 0.61017)$$

Figure 2.4: The equilibrium point $\bar{x} = (2, 5)^T$ when $b = 0.1$ is classified as an unstable node.

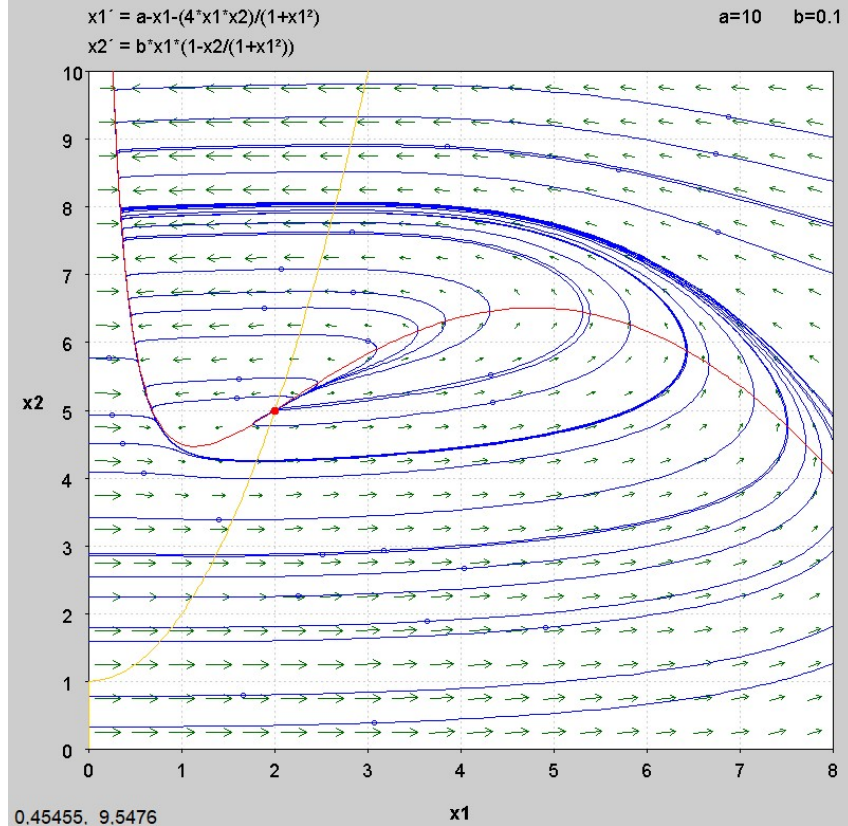


Figure 2.5: Phase Portrait of the System when $b = 0.1$. The equilibrium point $\bar{x} = (2, 5)^T$ is marked with a red dot, the nullclines are shown in red and yellow, and the trajectories are drawn in blue. The trajectories initially diverge from the equilibrium and then they are attracted to the stable limit cycle.

Case 2: $b = 2$

As shown in Fig. 2.6, the position of the equilibrium point remains unchanged at $\bar{x} = (2, 5)^T$. As far as the classification is concerned, it is a spiral. Additionally, the eigenvalues are complex and conjugate with both real parts positive, indicating that the equilibrium point is still unstable. Also in this case, the Poincarè-Bendixson theorem implies the existence of a closed orbit. For this reason, the trajectories firstly are repelled by definition of the unstable equilibrium, then they are attracted to the stable limit cycle [1], as shown in the phase portrait in Fig. 2.7.

Equilibrium Point:

There is a spiral source at $(2, 5)$

Jacobian:

$$\begin{matrix} 1,4 & -1,6 \\ 3,2 & -0,8 \end{matrix}$$

The eigenvalues and eigenvectors are:

$$\begin{matrix} 0,3+1,9774i & (-0,50454+0,28067i, 0+0,8165i) \\ 0,3-1,9774i & (0,50454+0,28067i, 0+0,8165i) \end{matrix}$$

Figure 2.6: The equilibrium point $\bar{x} = (2, 5)^T$ when $b = 2$ is classified as an unstable spiral.

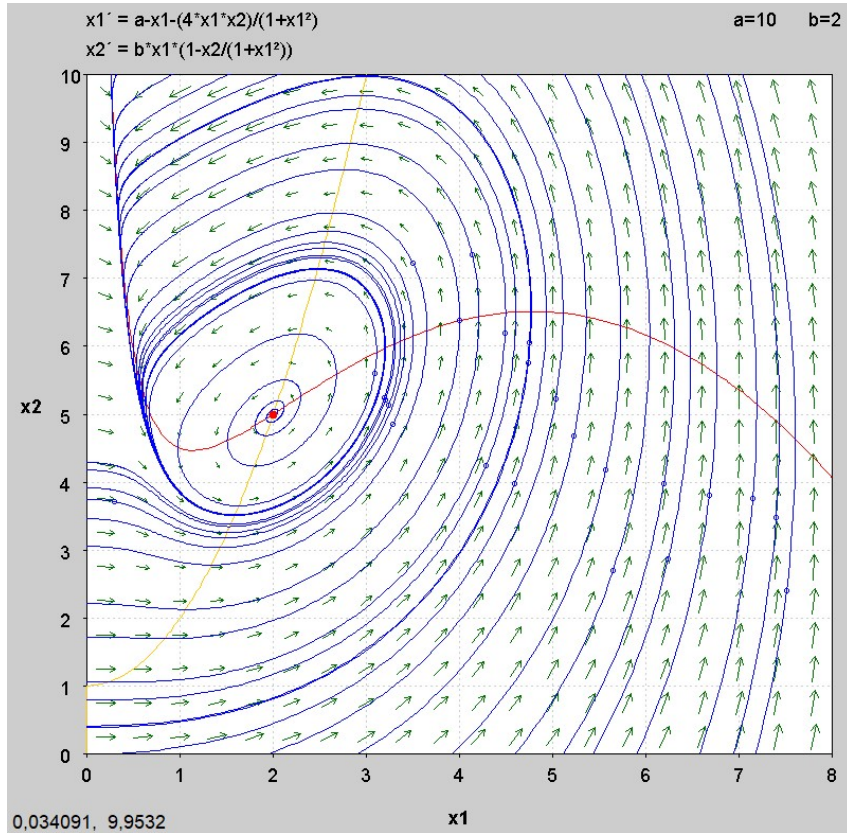


Figure 2.7: Phase Portrait of the System when $b = 2$. The equilibrium point $\bar{x} = (2, 5)^T$ is marked with a red dot, the nullclines are shown in red and yellow, and the trajectories are drawn in blue. The trajectories are firstly repelled by the unstable equilibrium, then they are attracted to the stable limit cycle.

Case 3: $b = 5$

As shown in Fig. 2.8, the position of the equilibrium point is still confirmed at $\bar{x} = (2, 5)^T$. As far as the classification is concerned, it is still a spiral, as expected. The eigenvalues are complex and conjugate with both real parts negative, indicating that the equilibrium point is stable. For this reason, all the trajectories spiral into the stable fixed point [1], as shown in the phase portrait in Fig. 2.9. Unlike the previous cases, the limit cycle doesn't exist anymore.

Equilibrium Point:

There is a spiral sink at $(2, 5)$

Jacobian:

$$\begin{array}{cc} 1,4 & -1,6 \\ 8 & -2 \end{array}$$

The eigenvalues and eigenvectors are:

$$\begin{array}{ll} -0,3+3,148i & (-0,35922+0,19399i, 0+0,91287i) \\ -0,3-3,148i & (0,35922+0,19399i, 0+0,91287i) \end{array}$$

Figure 2.8: The equilibrium point $\bar{x} = (2, 5)^T$ when $b = 5$ is classified as a stable spiral.

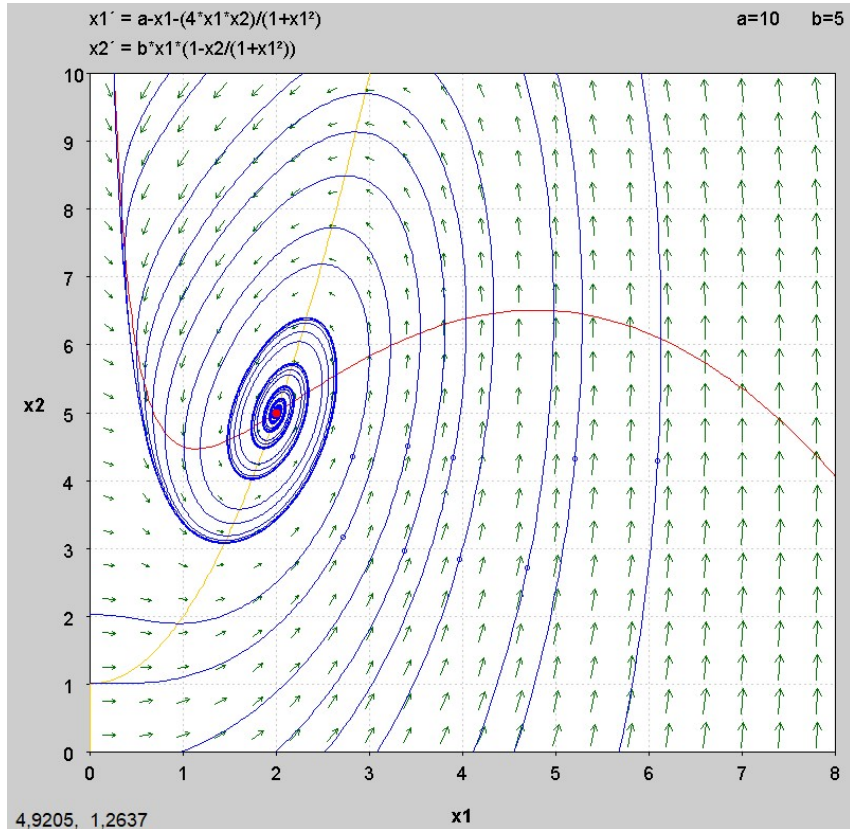


Figure 2.9: Phase Portrait of the System when $b = 5$. The equilibrium point $\bar{x} = (2, 5)^T$ is marked with a red dot, the nullclines are shown in red and yellow, and the trajectories are drawn in blue. The trajectories are attracted by the stable spiral.

As it is shown, there is a transition between Case 1 when $b = 0.1$ and Case 2 when $b = 2$ when the equilibrium passes from an unstable node to an unstable spiral, both surrounded by a stable limit cycle. As the previous analysis suggests, the transition occurs at $b = b_{c1} \approx 0.216$.

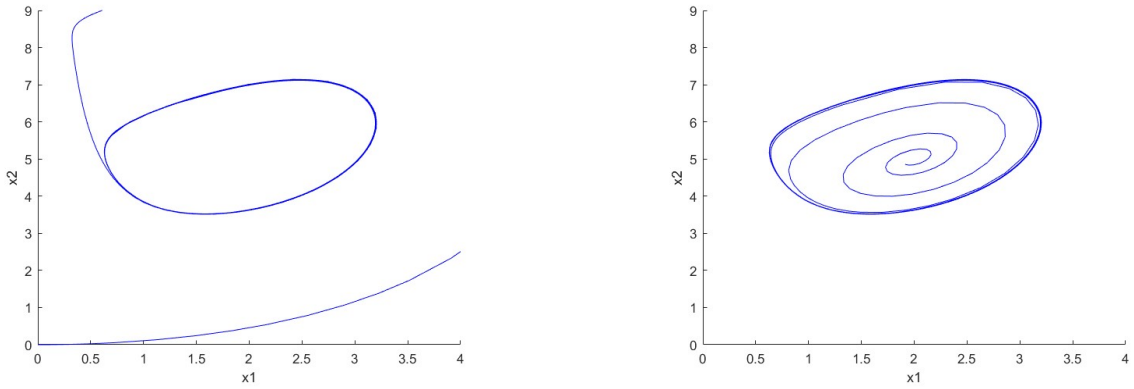
Then there is a transition between Case 2 when $b = 2$ and Case 3 when $b = 5$ when the equilibrium passes from the unstable spiral with a stable limit cycle to a stable spiral. This suggests the presence of a Hopf bifurcation. As the previous analysis suggests, the transition occurs at $b = b_{c2} = 3.5$.

2.3 Bifurcation Analysis

In order to verify the occurrence of any bifurcation, as discussed in the previous section, the MATLAB software MatCont is used [5].

First of all, the system is analyzed for two different values of the parameter, specifically $b = 2$ and $b = 5$, to better visualize the limit cycle.

For the first simulation, shown in Fig. 2.10, two different initial conditions are chosen: in Fig. 2.10a the initial condition is set to $x_{01} = (0, 0)^T$, while in Fig. 2.10b the initial condition is set to $x_{02} = (1.9, 4.9)^T$. In both cases, the trajectory is attracted to the stable limit cycle, which its presence is already discussed, but in this scenario is more visible.



(a) Trajectory of the system when $b = 2$
with $x_{01} = (0, 0)^T$

(b) Trajectory of the system when $b = 2$
with $x_{02} = (1.9, 4.9)^T$

Figure 2.10: Comparison of system trajectories when $b = 2$ with different initial conditions x_{01} and x_{02} . In both cases, the trajectories are attracted to the stable limit cycle

In this second simulation, for $b = 5$, the initial condition is set to $x_{01} = (0, 0)^T$. In this case, the trajectory converges to the equilibrium point \bar{x} , confirming its stability and the absence of the limit cycle, as shown in Fig. 2.11.

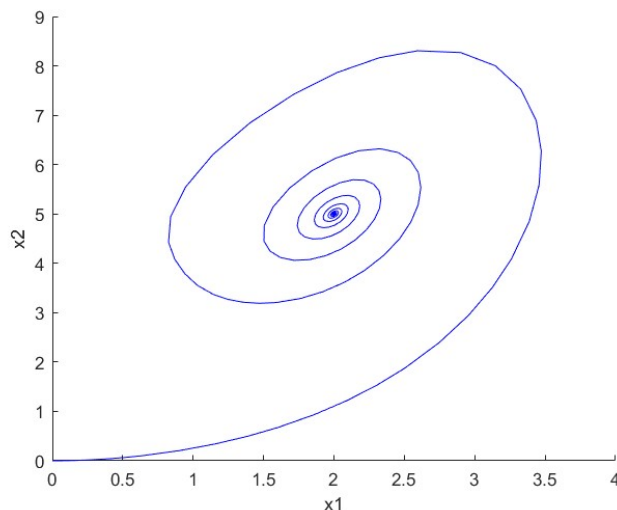


Figure 2.11: Trajectory of the system when $b = 5$ with $x_{01} = (0, 0)^T$. The trajectory goes to the stable equilibrium point $\bar{x} = (2, 5)^T$

For the bifurcation analysis in MatCont, the parameter b is varied. As shown in Fig. 2.12, MatCont reveals that an Hopf bifurcation occurs.

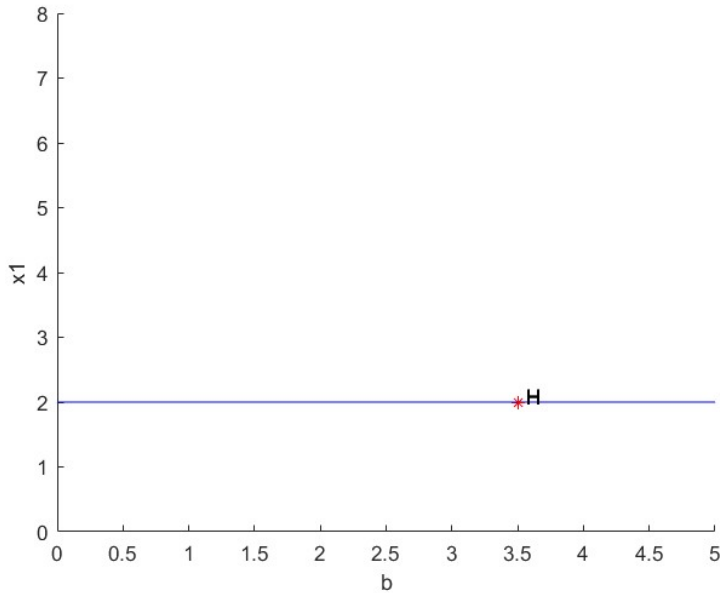


Figure 2.12: Bifurcation diagram varying b . MatCont confirms the occurrence of a Hopf bifurcation.

Additionally, in Fig. 2.13 the bifurcation point is confirmed at $b = b_{c2} = 3.5$, consistent with the previous analysis.

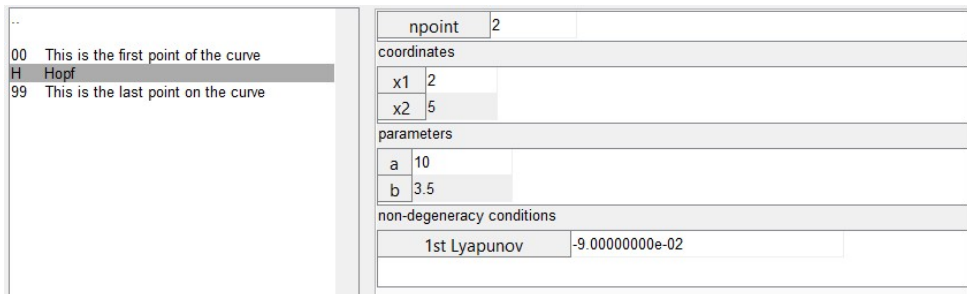


Figure 2.13: Detail of the bifurcation analysis in MatCont, confirming the Hopf bifurcation occurs at $b = b_{c2} = 3.5$.

In this case, the Hopf bifurcation is supercritical [1] because after the fixed point loses stability, it is surrounded by a stable limit cycle.

At the end, since the presence of a limit cycle for $b < b_{c2} = 3.5$ has been identified in the previous analysis, in Fig. 2.14 is analyzed its amplitude. Specifically, as $b \rightarrow b_{c2}$ from 0, the limit cycle gradually shrinks and converges to the bifurcation point.

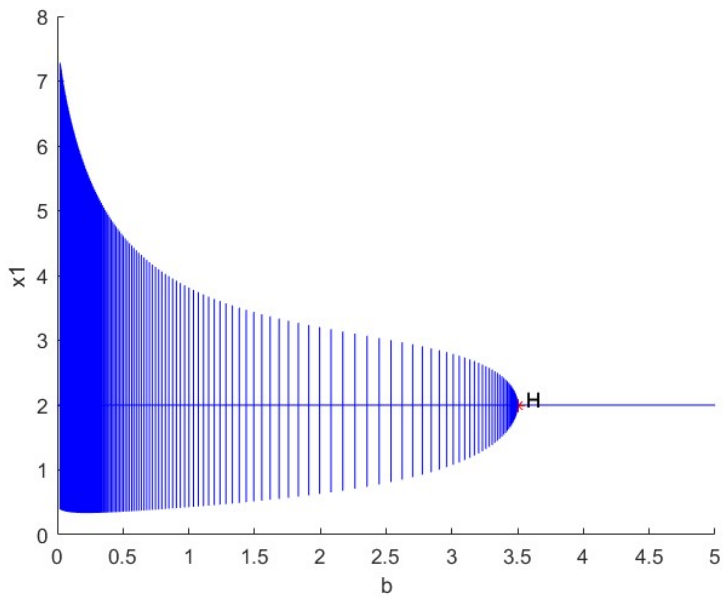


Figure 2.14: Analysis of the amplitude of the limit cycle that occurs for $b < b_{c2} = 3.5$

Chapter 3

Control Synthesis

The model in (1.6), with $a = 10$ and $b = 2$, is simulated without any control action with $x_0 = (2.5, 5.2)^T$. The state trajectories keep oscillating around the equilibrium point since it is an unstable spiral surrounded by a stable limit cycle, as shown in Fig. 3.1. A control strategy is necessary to stabilize the system and ensure that the state converges to the desired reference with the desired specifications.

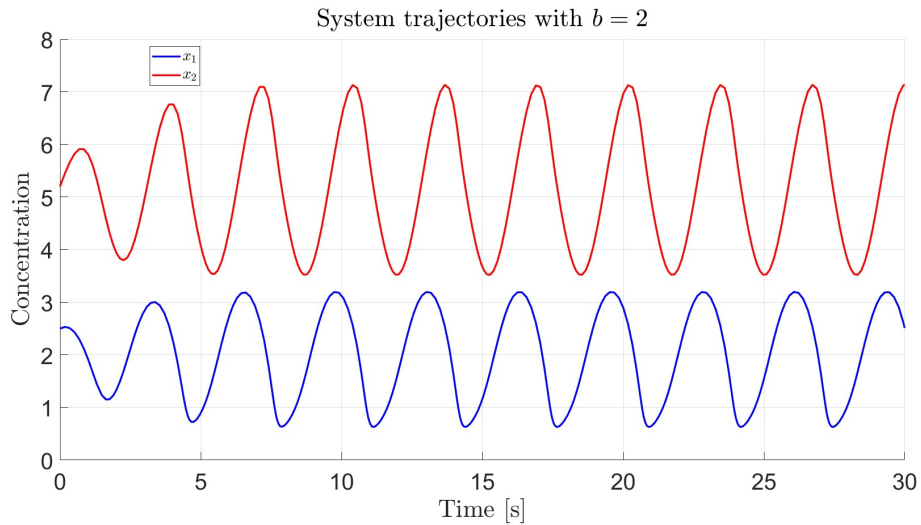


Figure 3.1: State trajectories in free evolution with $x_0 = (2.5, 5.2)^T$

In order to regulate the CIMA reaction, a control input u is introduced to act on the concentrations of the reactants. In this case, the model (1.6) is rewritten as follows:

$$\dot{x}_1 = a - x_1 - \frac{4x_1x_2}{1 + x_1^2} + u \quad (3.1a)$$

$$\dot{x}_2 = b \left(x_1 - \frac{x_1x_2}{1 + x_1^2} \right) \quad (3.1b)$$

Specifically, the control input u is introduced to regulate the concentration of iodide (I^-) in the system. This can be achieved by using a peristaltic pump, whose dynamics is neglected in the model. Since the model's variable are scaled as in (1.4), the control input can be expressed dimensionless as:

$$u = U \frac{\gamma}{\alpha} \quad (3.2)$$

where U is the physically dimensional control action. Since the control input corresponds to a reactant introduced by a peristaltic pump, it is only possible to increase the concentration of the reactant. Indeed, during the reaction, the concentrations are mixed, making it very difficult to remove a single reactant without interfering with the others. This means that u must be non-negative.

The objective of the control synthesis is to regulate the concentration of iodide:

$$y = x_1 \quad (3.3)$$

For this purpose, three different controllers have been implemented, one linear and two nonlinear:

1. Linear LQ Optimal Control
2. I/O Feedback Linearization Control
3. Sliding Mode Control

Specifically, the aim of each controller is to track two types of desired reference signals:

- Constant reference $x_{1d} = 5$;
- Sinusoidal reference $x_{1d} = 5 + A_d \sin(\omega_d t)$ with $A_d = [0.2 \quad 0.5]$ and $\omega_d = [0.5 \quad 2]$;

while ensuring that the following specifications are met:

- Steady state error $|e_\infty| \leq 1\%$;
- 1% Settling time $t_{s,1\%} \leq 5s$;
- Bounded control input $0 \leq u \leq 20$;

The initial condition for each controller is set near the equilibrium point as follows:

$$x_0 = \begin{bmatrix} \bar{x}_1 + 0.5 \\ \bar{x}_2 + 0.2 \end{bmatrix} = \begin{bmatrix} 2.5 \\ 5.2 \end{bmatrix} \quad (3.4)$$

3.1 Linear LQ Optimal Control

The Linear Quadratic (LQ) Optimal Control is a widely used linear control technique. Since the model in (3.1) is nonlinear, it's necessary to compute the linearized model around an equilibrium point. The equilibrium point is $\bar{x} = (2, 5)^T$ and, setting $\bar{u} = 0$, it is obtain the linearized system:

$$\delta \dot{x} = A \delta x + B \delta u \quad (3.5a)$$

$$\delta y = C \delta x + D \delta u \quad (3.5b)$$

where:

$$\delta x = x - \bar{x}, \quad \delta u = u - \bar{u} = u. \quad (3.6)$$

The linearized system matrices are:

$$A = \frac{\partial f(x)}{\partial x} \Big|_{(\bar{x}, \bar{u})} = \begin{bmatrix} 1.4 & -1.6 \\ 3.2 & -0.8 \end{bmatrix} \quad (3.7a)$$

$$B = \frac{\partial f(x)}{\partial u} \Big|_{(\bar{x}, \bar{u})} = \begin{bmatrix} 1 \\ 0 \end{bmatrix} \quad (3.7b)$$

The output matrices C and D are chosen as:

$$C = \begin{bmatrix} 1 & 0 \\ 0 & 1 \end{bmatrix} \quad (3.8a)$$

$$D = \begin{bmatrix} 0 \\ 0 \end{bmatrix} \quad (3.8b)$$

The LQ Optimal Control computes the state-feedback control law:

$$u = -Kx \quad (3.9)$$

In particular, the feedback matrix K is selected to minimize the quadratic cost function:

$$J = \int_0^{+\infty} (x^T Q x + u^T R u) dt \quad (3.10)$$

The matrices Q and R are used to weight the state variables and the control input, respectively. A higher weight implies greater priority in the minimization process, leading to stronger minimization of the corresponding variable. To ensure a meaningful cost function, the weight matrices must satisfy $Q \geq 0$ and $R > 0$. A typical approach for select Q and R is trial and error guided by the desired specification.

Since state feedback alone does not ensure zero steady-state error and robustness to model uncertainties, an integral action is applied to the error

$$\delta \dot{x}_i = y_{1d} - y = x_{1d} - x_1 \quad (3.11)$$

This allows the augmented system dynamics to be expressed as

$$\begin{bmatrix} \delta \dot{x} \\ \delta \dot{x}_i \end{bmatrix} = A_{aug} \begin{bmatrix} \delta x \\ \delta x_i \end{bmatrix} + B_{aug} \delta u + \begin{bmatrix} 0 \\ x_{1d} \end{bmatrix} \quad (3.12)$$

In this way, the augmented matrices are:

$$A_{aug} = \begin{bmatrix} A & 0 \\ -c & 0 \end{bmatrix}, \quad B_{aug} = \begin{bmatrix} B \\ 0 \end{bmatrix}, \quad C_{aug} = [C \ 0_{2 \times 1}], \quad D_{aug} = D \quad (3.13)$$

where $c = [1 \ 0]$ since the integral action is applied only on x_1 .

The optimal feedback gain K with the integral action is now composed of two parts: one related to the state feedback K_p and another one related to the integral action K_i .

The resulting control law is:

$$u = -K_p \delta x - K_i \int_0^{+\infty} (x_{1d}(t) - x_1(t)) dt \quad (3.14)$$

The weight matrices are chosen as:

$$Q = diag([800, 10, 10000]), \quad R = 100 \quad (3.15)$$

To ensure the stability of the closed-loop system, the following conditions must be verified:

- the pair (A_{aug}, B_{aug}) is completely controllable;
- the pair (A_{aug}, M) is completely observable with $M^T M = Q$.

Since these conditions are satisfied, the closed-loop matrix $A_{aug} - B_{aug}K$ is guaranteed to be asymptotically stable. Thanks to this choice, it is possible to compute K using the MATLAB command [6]:

$$\begin{bmatrix} K_{p1} & K_{p2} & K_i \end{bmatrix} = \text{lqr}(A_{aug}, B_{aug}, Q, R) = \begin{bmatrix} 6.0085 & -1.3628 & -10.0000 \end{bmatrix} \quad (3.16)$$

Once the LQ controller design is done onto the linearized system, the resulting control input is tested on the nonlinear system using the Simulink scheme in Fig. 3.2.

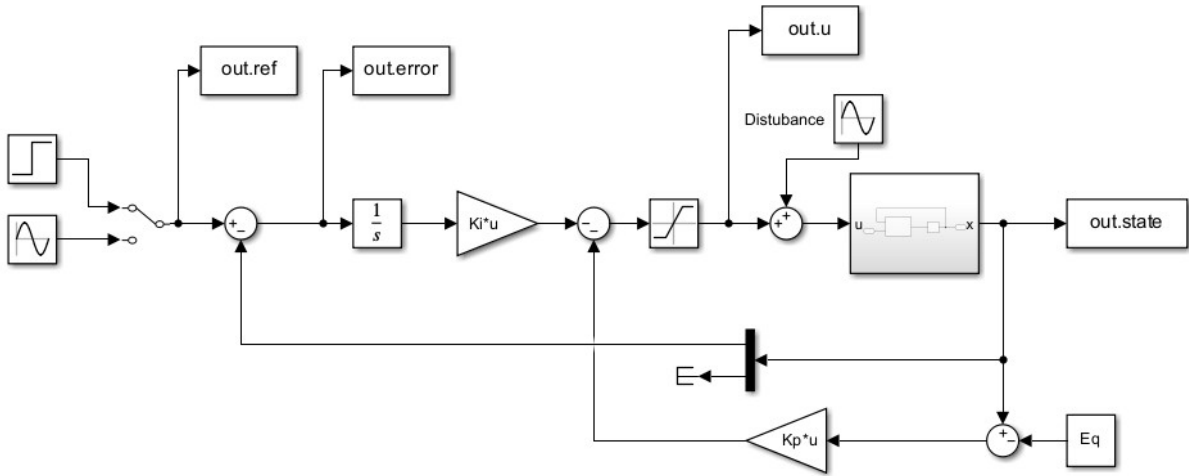


Figure 3.2: Control Scheme with the LQ Optimal Controller

The first simulation is performed using a constant reference. As shown in Fig. 3.3-3.5, the output successfully reaches the desired reference, and the performance specifications are achieved as follows:

- Steady-state error: $|e_\infty| = 0.01\%$;
- Settling time 1%: $t_{s,1\%} \approx 5$ s;
- Maximum control input: $\|u\|_\infty = 15$.

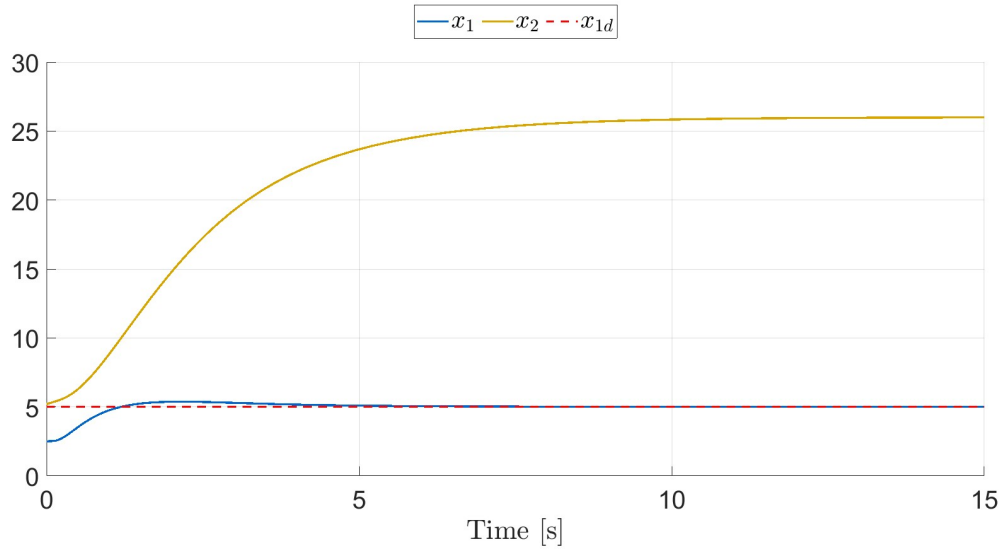


Figure 3.3: State Trajectories using LQ Controller with $x_{1d} = 5$, without parametric uncertainties or disturbances.

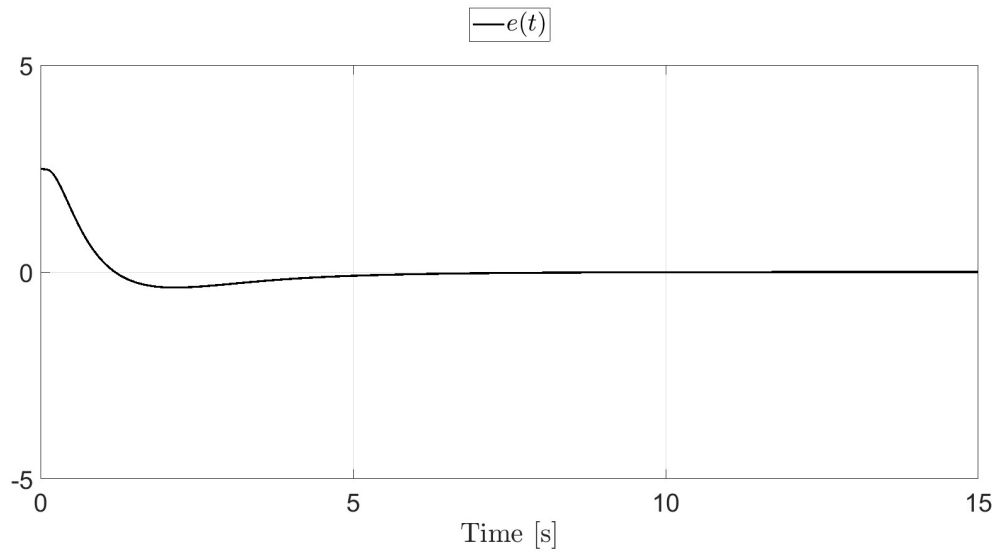


Figure 3.4: Error evolution $e = x_{1d} - x_1$ using LQ Controller with $x_{1d} = 5$, without parametric uncertainties or disturbances.

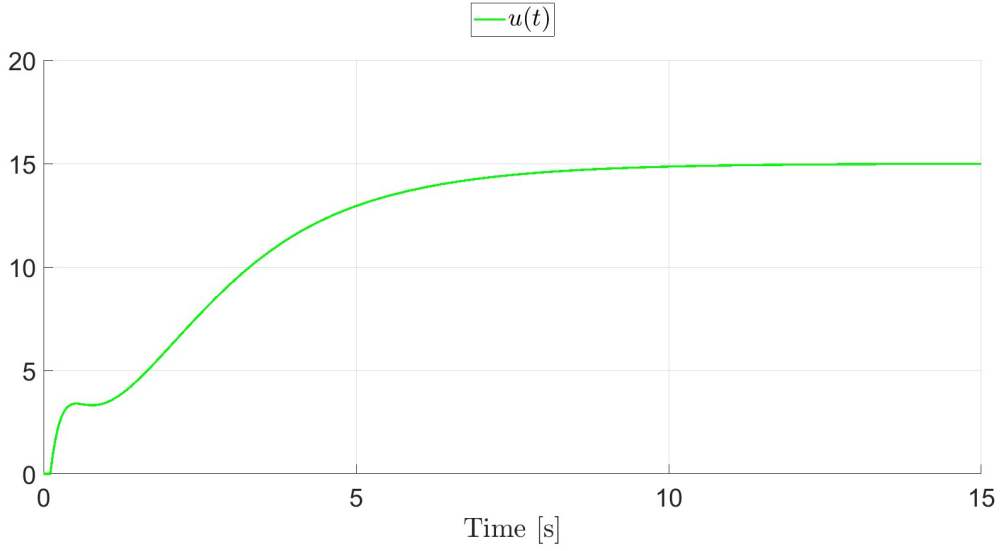


Figure 3.5: Control Input using LQ Controller with $x_{1d} = 5$, without parametric uncertainties or disturbances.

The system is now tested with a sinusoidal reference input. The results shown in the following figures indicate that the LQ controller effectively tracks low-frequency sinusoidal references, even with larger amplitudes, with a minimal steady-state error. Specifically, in Fig. 3.6 and Fig. 3.10, the steady-state error is $|e_\infty| = 0.78\%$ and $|e_\infty| = 2\%$, respectively. However, as the frequency increases, as in Fig. 3.8 and Fig. 3.12, the system exhibits a significant increase in steady-state error and a longer settling time. Despite these variations, in all simulations, the control input remains within the specified bounds.

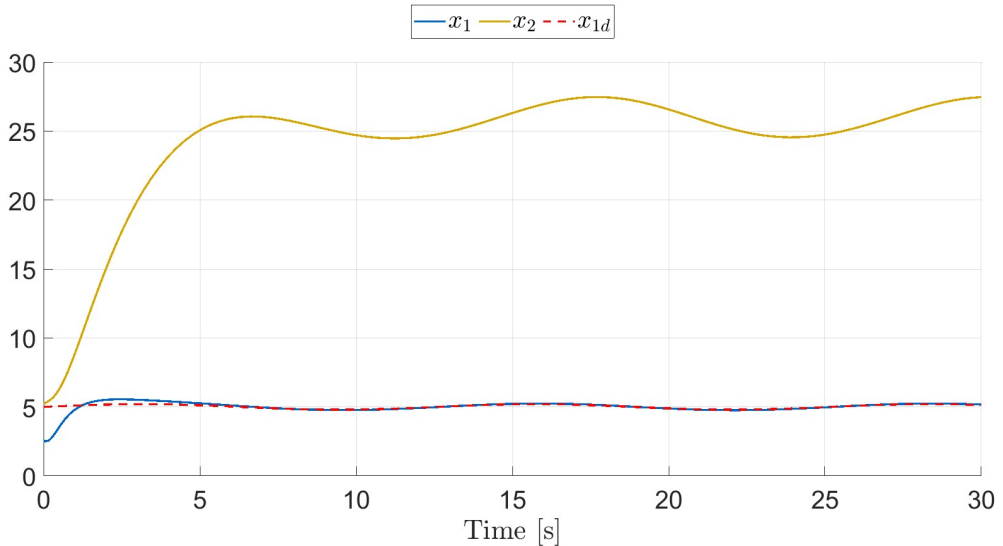


Figure 3.6: State Trajectories using LQ Controller with $x_{1d} = 5 + 0.2\sin(0.5t)$, without parametric uncertainties or disturbances.

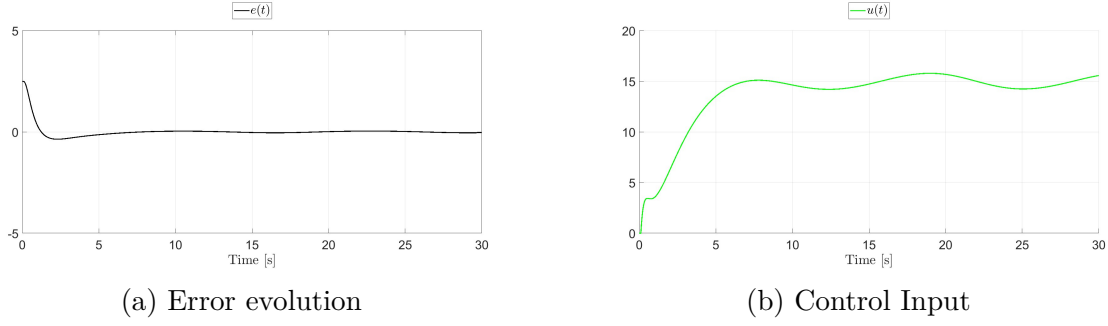


Figure 3.7: Error evolution (a) and Control Input (b) using LQ Controller with $x_{1d} = 5 + 0.2\sin(0.5t)$, without parametric uncertainties or disturbances.

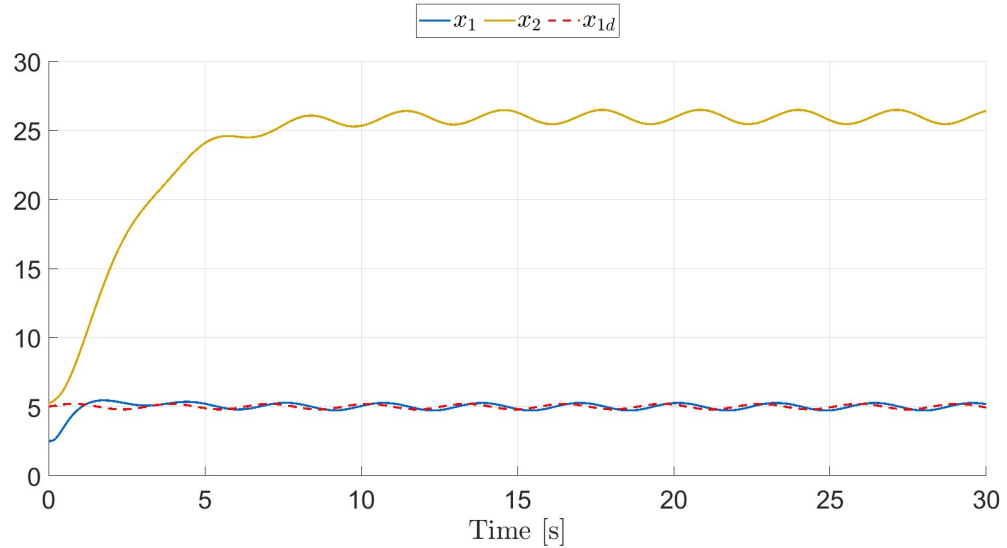


Figure 3.8: State Trajectories using LQ Controller with $x_{1d} = 5 + 0.2\sin(2t)$, without parametric uncertainties or disturbances.

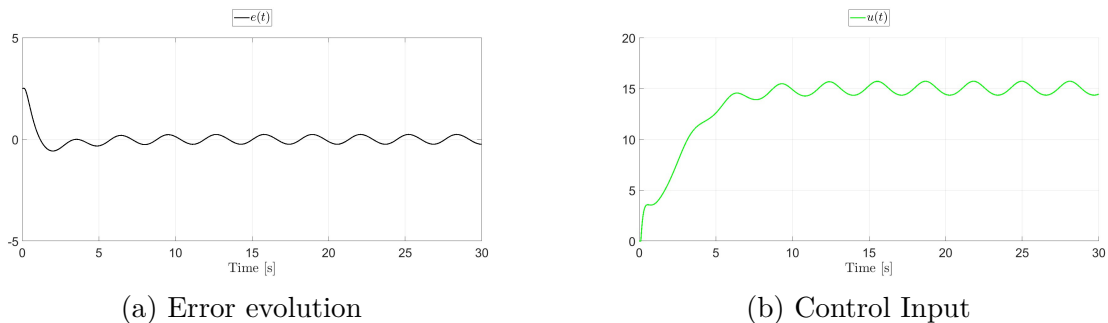


Figure 3.9: Error evolution (a) and Control Input (b) using LQ Controller with $x_{1d} = 5 + 0.2\sin(2t)$, without parametric uncertainties or disturbances.

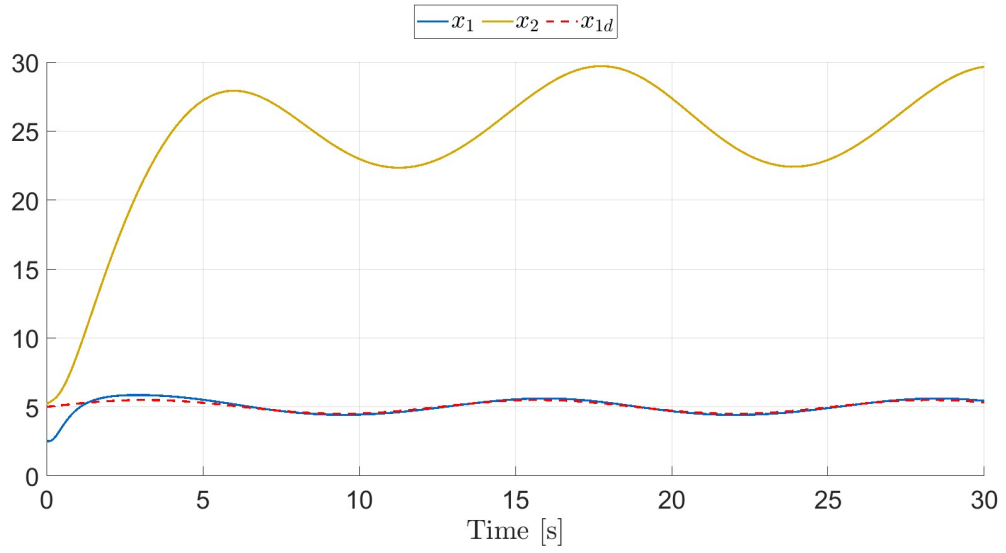


Figure 3.10: State Trajectories using LQ Controller with $x_{1d} = 5 + 0.5\sin(0.5t)$, without parametric uncertainties or disturbances.

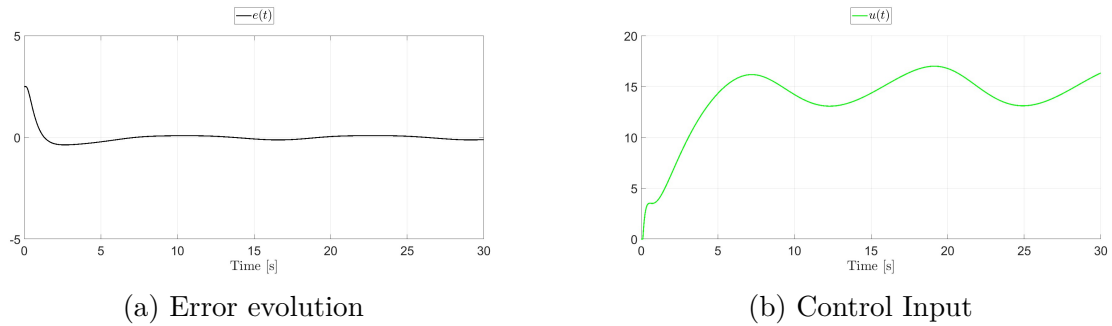


Figure 3.11: Error evolution (a) and Control Input (b) using LQ Controller with $x_{1d} = 5 + 0.5\sin(0.5t)$, without parametric uncertainties or disturbances.

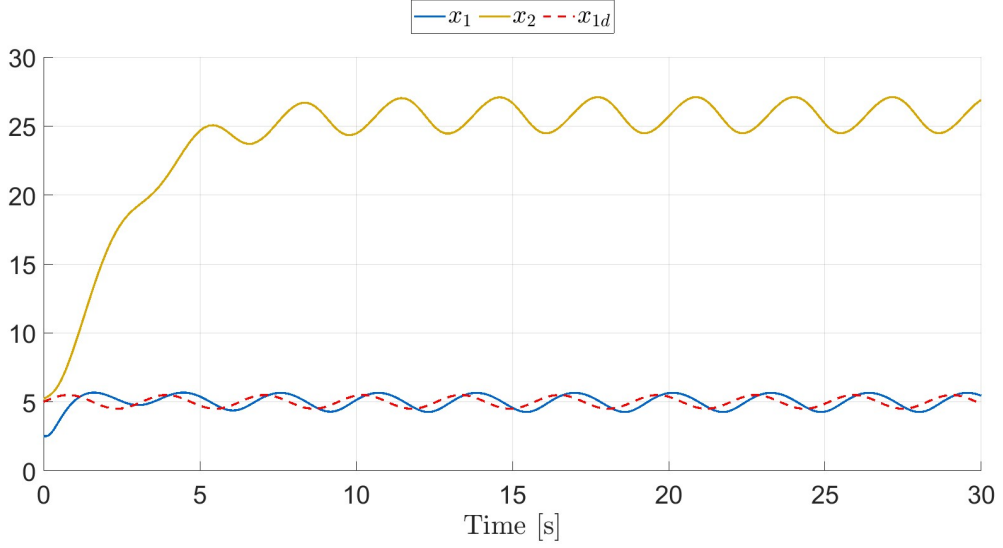


Figure 3.12: State Trajectories using LQ Controller with $x_{1d} = 5 + 0.5\sin(2t)$, without parametric uncertainties or disturbances.

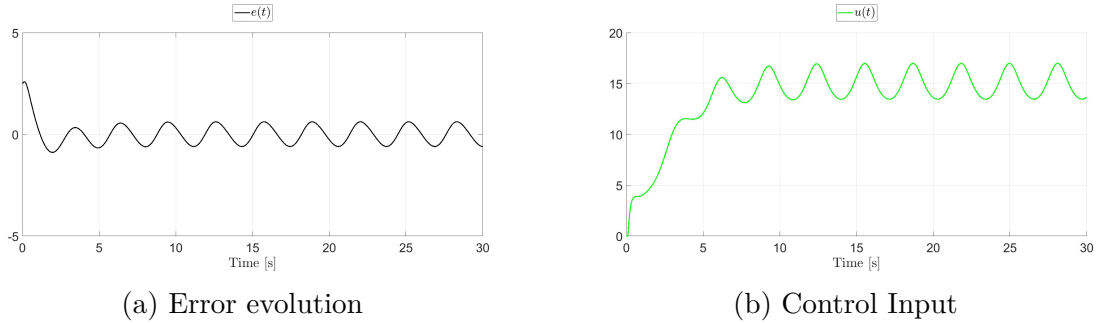


Figure 3.13: Error evolution (a) and Control Input (b) using LQ Controller with $x_{1d} = 5 + 0.5\sin(2t)$, without parametric uncertainties or disturbances.

3.2 I/O Feedback Linearization

Input/Output (I/O) Feedback Linearization is a nonlinear control technique that belongs to the class of geometric control approaches. The goal of feedback linearization is to design a nonlinear control law $u = u(x, t)$ capable of transforming the original nonlinear system into an I/O linear system, described by the input-output equation:

$$y^{(r)} = v \quad (3.17)$$

where r is the relative degree of the system and v is the auxiliary control input. To design the controller, the system must be expressed in its affine form:

$$\begin{aligned} \dot{x} &= f(x) + g(u) \\ y &= h(x) \end{aligned} \quad (3.18)$$

For the CIMA system, the functions are defined as:

$$f(x) = \begin{bmatrix} a - x_1 - \frac{4x_1x_2}{1+x_1^2} \\ bx_1 \left(1 - \frac{x_2}{1+x_1^2}\right) \end{bmatrix} \quad (3.19a)$$

$$g(x) = \begin{bmatrix} 1 \\ 0 \end{bmatrix} \quad (3.19b)$$

$$h(x) = x_1 \quad (3.19c)$$

To compute the relative degree r , it is necessary to compute the Lie derivative of $h(x)$ with respect to $g(x)$:

$$\mathcal{L}_g(h) = \nabla h \cdot g = \begin{bmatrix} 1 & 0 \end{bmatrix} \begin{bmatrix} 1 \\ 0 \end{bmatrix} = 1 \quad (3.20)$$

Since $\mathcal{L}_g(h) \neq 0$, the relative degree is $r = 1$, so the input output relationship of the linearized system is:

$$\dot{y} = v \quad (3.21)$$

The feedback linearized control input is given by:

$$u = \frac{1}{\mathcal{L}_g(\mathcal{L}_f^{r-1}(h))} [v - \mathcal{L}_f^r(h)] \quad (3.22)$$

where:

$$\mathcal{L}_f(h) = \nabla h \cdot f = \begin{bmatrix} 1 & 0 \end{bmatrix} f = a - x_1 - \frac{4x_1x_2}{1+x_1^2} \quad (3.23)$$

Thus, the explicit expression for u is:

$$u = v - a + x + \frac{4x_1x_2}{1+x_1^2} \quad (3.24)$$

It's possible to express v in terms of the error $e = x_{1d} - x_1$, where x_{1d} is the desired reference trajectory:

$$v = -\dot{x}_{1d} + K_p(x_{1d} - x_1) + K_i \int_0^{+\infty} (x_{1d}(t) - x_1(t)) dt \quad (3.25)$$

By choosing $K_p > 0$ and $K_i > 0$, the error dynamics converges asymptotically to 0.

Before simulating the designed controller, it is important to analyze the internal dynamics. Given that $r = 1$ is less than $n = 2$ an internal dynamic remains, which is not directly considered in the linearized system. It is necessary to verify that the internal dynamics is at least Bounded-Input Bounded-Output (BIBO) stable, otherwise the feedback linearization approach becomes meaningless. Since $b = 2 > 0$, the internal dynamics is BIBO stable. In fact with the zero dynamics, if $\dot{x}_1 = 0$ means that x_1 is a constant, positive by definition. Fixing x_1 at a constant positive value, the dynamics of x_2 from (3.1b) simplifies to:

$$\dot{y} = bx_{\text{const}} - \frac{bx_{\text{const}}}{1+x_{\text{const}}^2} y$$

which represents a stable linear system with a constant forcing term, confirming that the internal dynamics does not introduce instability.

Choosing $K_p = 4$ and $K_i = 0.5$, the Simulink scheme implementing the Feedback Linearization controller is shown in Fig. 3.14.

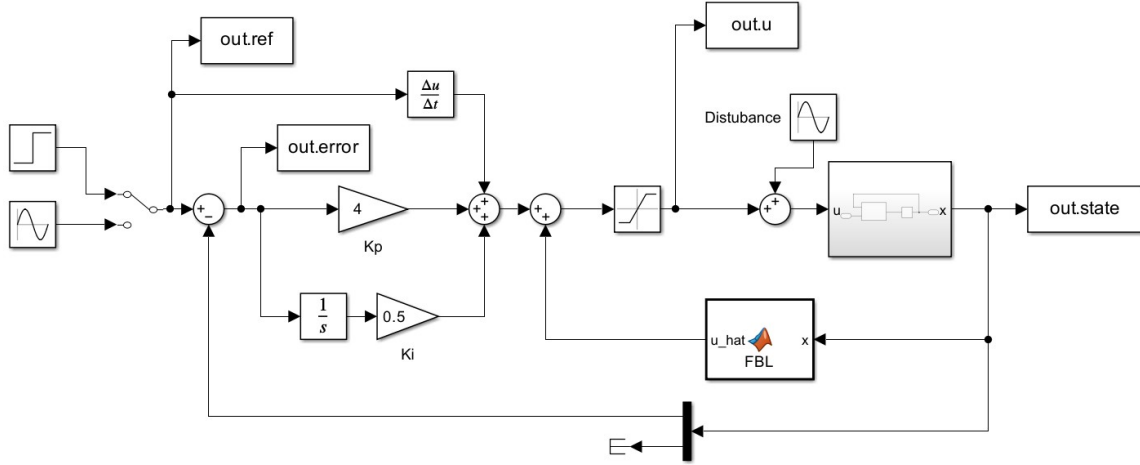


Figure 3.14: Control Scheme with the I/O Feedback Linearization Controller.

The first simulation is performed using a constant reference. As shown in Fig. 3.15-3.17, the output successfully reaches the desired reference, and the performance specifications are achieved as follows:

- Steady-state error: $|e_\infty| = 0.04\%$;
- Settling time 1%: $t_{s,1\%} \approx 4$ s;
- Maximum control input: $\|u\|_\infty = 15$.

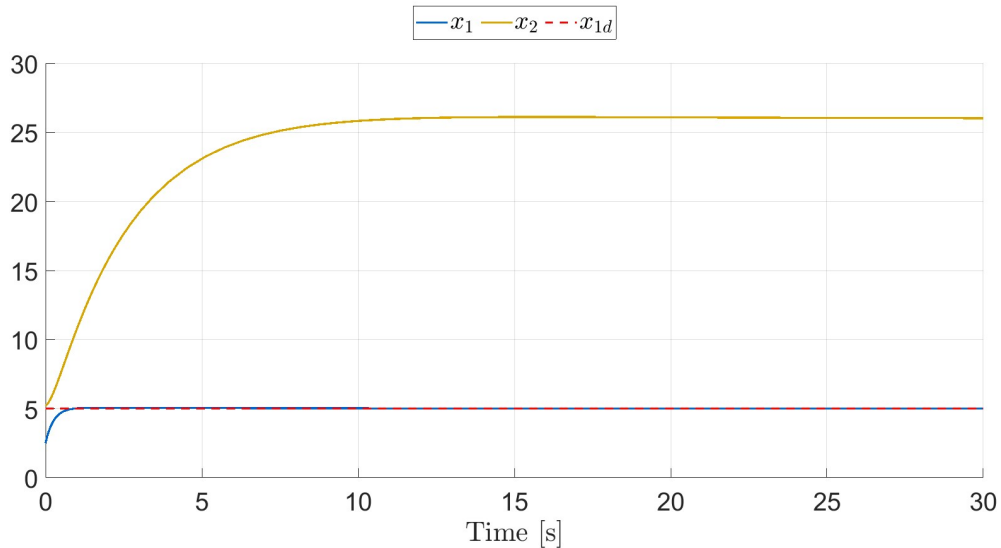


Figure 3.15: State Trajectories using FBL Controller with $x_{1d} = 5$, without parametric uncertainties or disturbances.

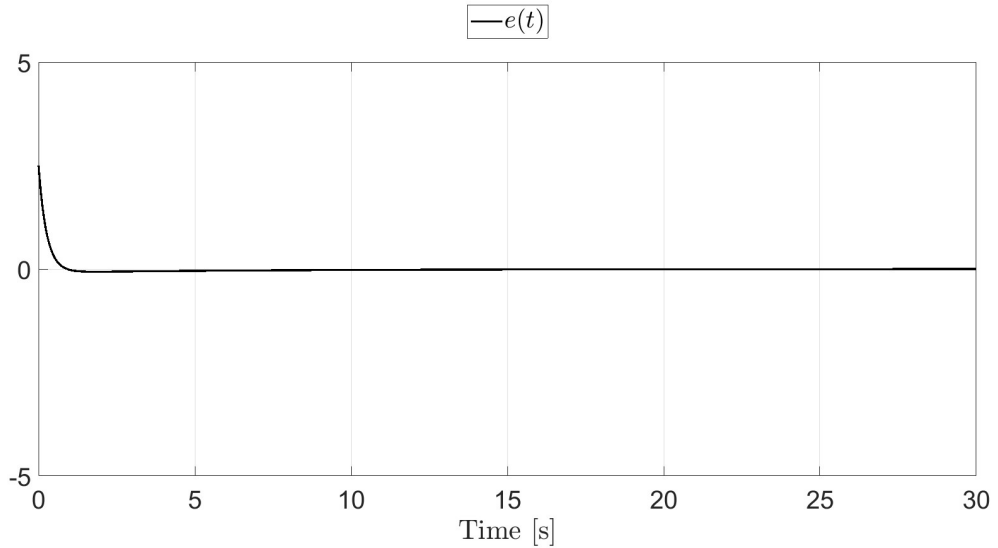


Figure 3.16: Error evolution $e = x_{1d} - x_1$ using FBL Controller with $x_{1d} = 5$, without parametric uncertainties or disturbances.

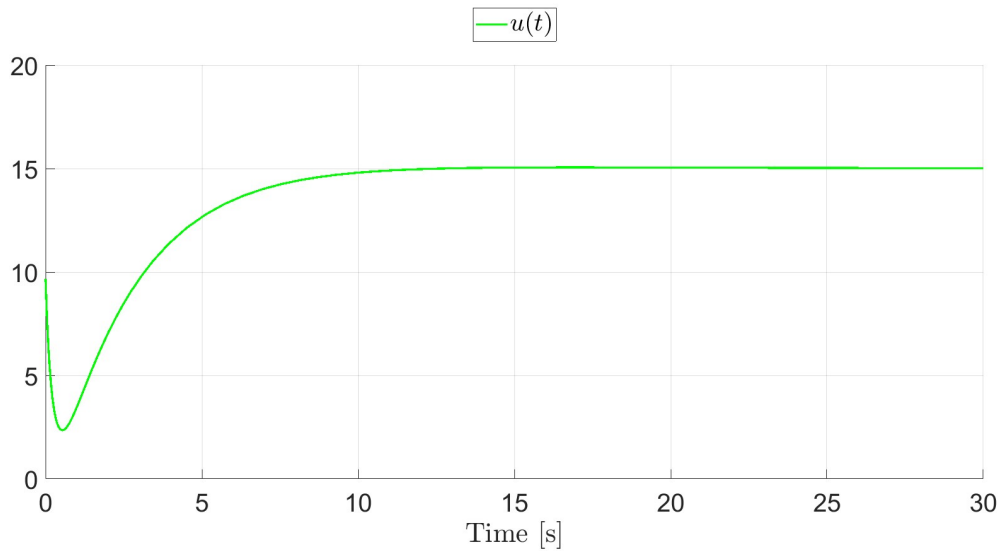


Figure 3.17: Control Input using FBL Controller with $x_{1d} = 5$, without parametric uncertainties or disturbances.

The system is now tested with a sinusoidal reference input. The results shown in the following figures indicate that the FBL controller effectively tracks both low and high frequency sinusoidal references, even with larger amplitudes, with minimal steady-state error and fast settling time. In all simulations, the steady-state error remains around $|e_\infty| = 0.04\%$, while the settling time is approximately $t_{s,1\%} \approx 5s$.

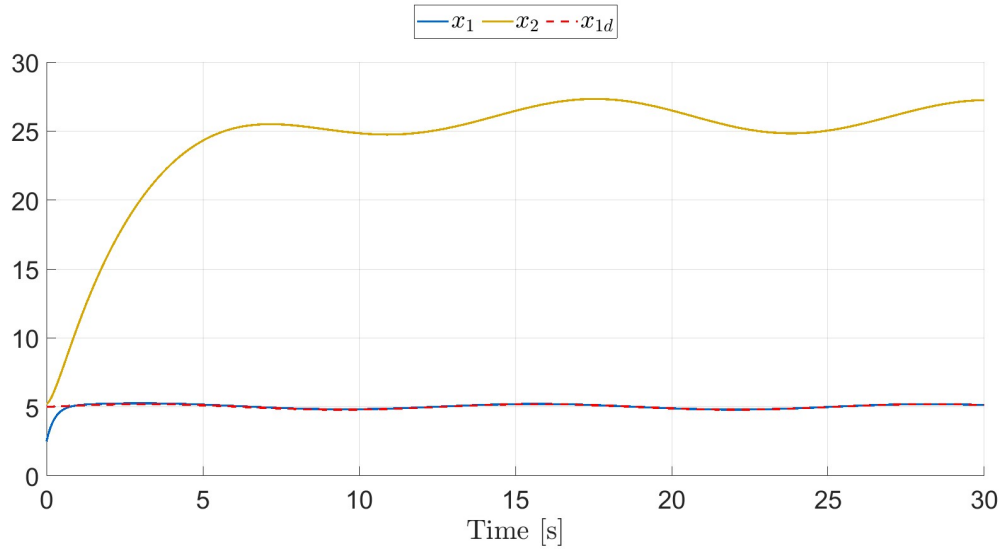


Figure 3.18: State Trajectories using FBL Controller with $x_{1d} = 5 + 0.2 \sin(0.5t)$, without parametric uncertainties or disturbances.

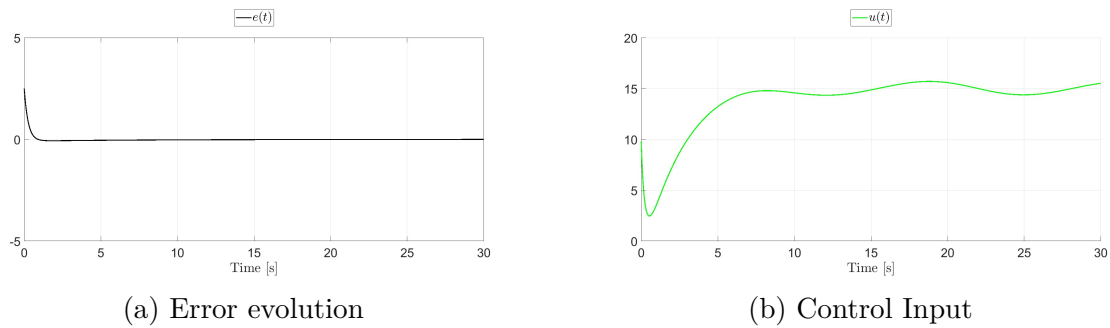


Figure 3.19: Error evolution (a) and Control Input (b) using FBL Controller with $x_{1d} = 5 + 0.2 \sin(0.5t)$, without parametric uncertainties or disturbances.

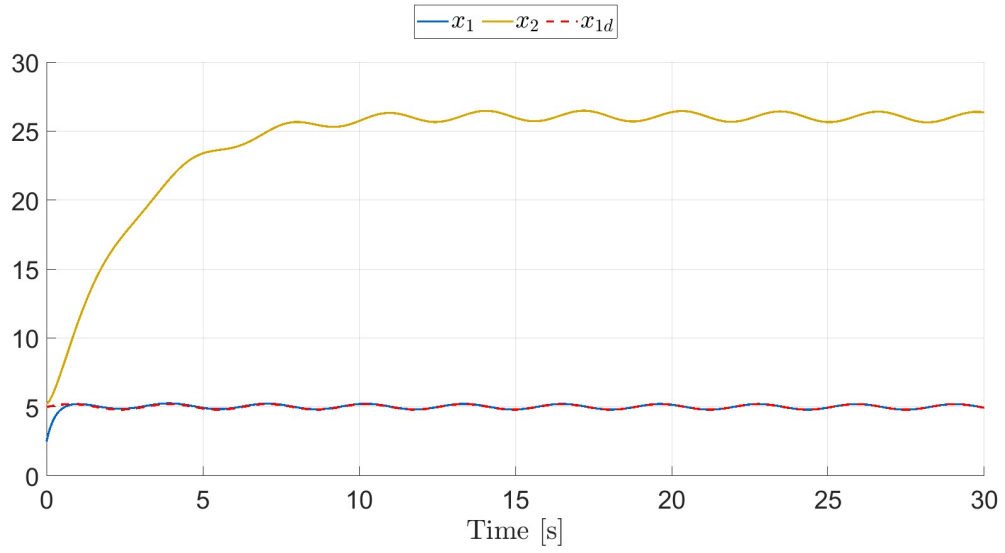


Figure 3.20: State Trajectories using FBL Controller with $x_{1d} = 5 + 0.2 \sin(2t)$, without parametric uncertainties or disturbances.

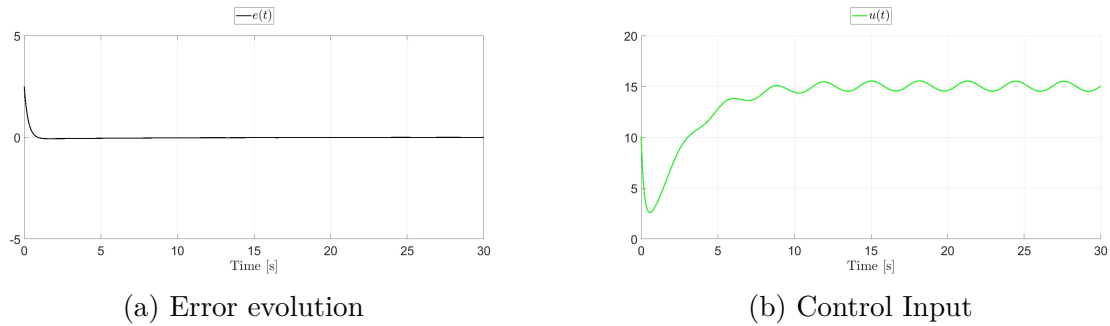


Figure 3.21: Error evolution (a) and Control Input (b) using FBL Controller with $x_{1d} = 5 + 0.2 \sin(2t)$, without parametric uncertainties or disturbances.

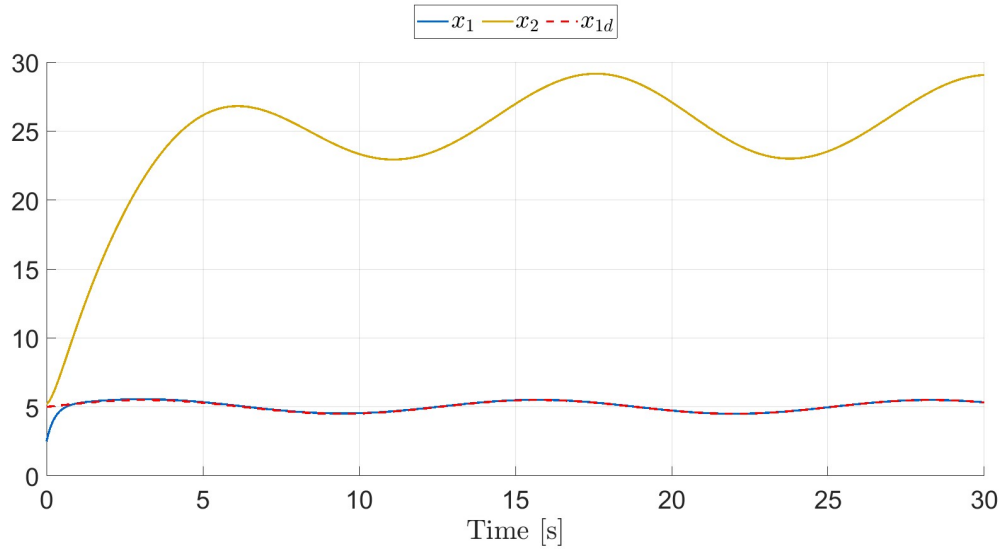


Figure 3.22: State Trajectories using FBL Controller with $x_{1d} = 5 + 0.5 \sin(0.5t)$, without parametric uncertainties or disturbances.

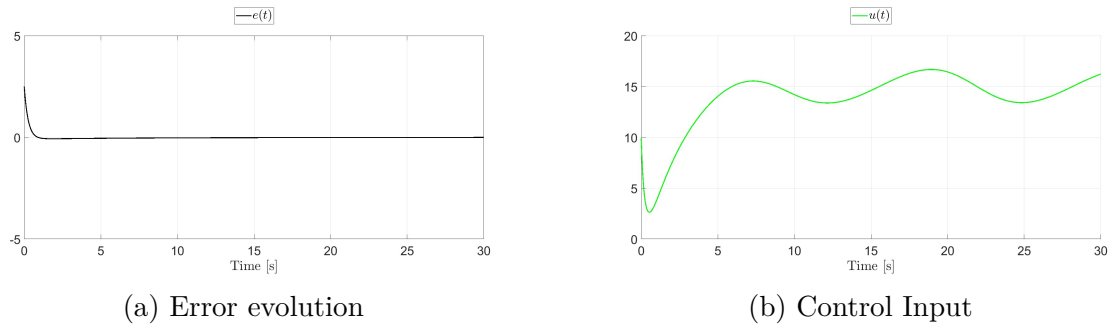


Figure 3.23: Error evolution (a) and Control Input (b) using FBL Controller with $x_{1d} = 5 + 0.5 \sin(0.5t)$, without parametric uncertainties or disturbances.

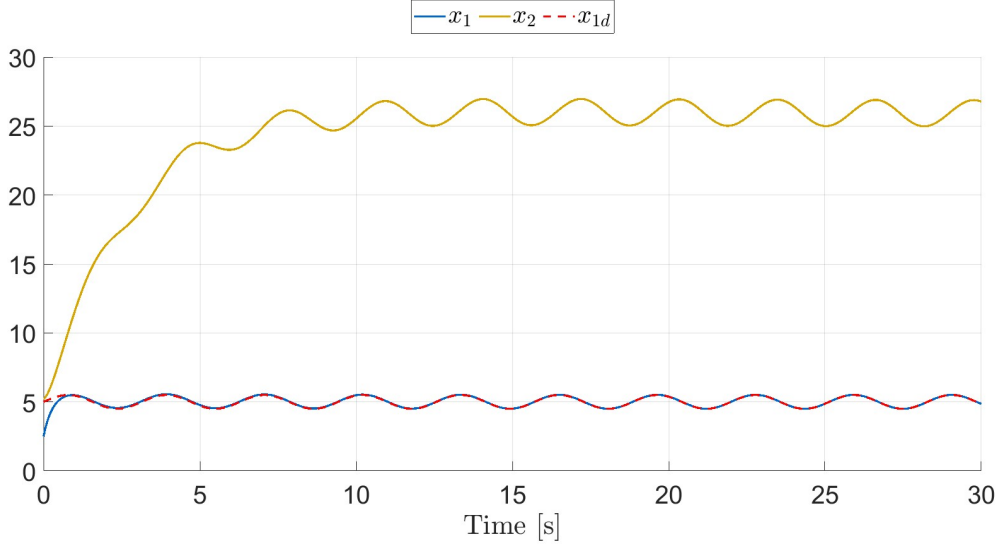


Figure 3.24: State Trajectories using FBL Controller with $x_{1d} = 5 + 0.5 \sin(2t)$, without parametric uncertainties or disturbances.

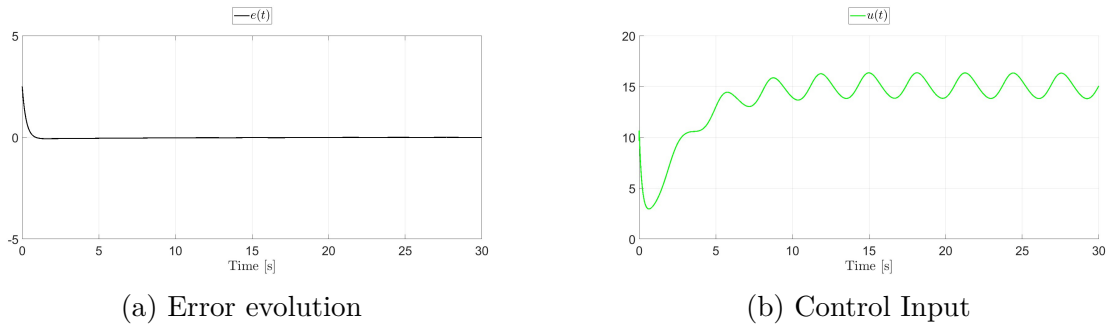


Figure 3.25: Error evolution (a) and Control Input (b) using FBL Controller with $x_{1d} = 5 + 0.5 \sin(2t)$, without parametric uncertainties or disturbances.

3.3 Sliding Mode Control

The Sliding Mode Control (SMC) is a nonlinear control technique based on the idea that the structure of the controller changes dynamically depending on specific conditions. This approach forces the state trajectories onto a predefined surface, ensuring that the desired performance specifications are met while maintaining robustness against disturbances and uncertainties. To achieve this, a switching function $\sigma(x) : \mathbb{R}^n \rightarrow \mathbb{R}$ is selected to define the sliding surface $\Sigma := \{x \in \mathbb{R}^n \mid \sigma(x) = 0\}$. Once the trajectory reaches this surface, the system dynamics are constrained to remain on it, achieving sliding motion.

Considering the affine system representation given in (3.19), the switching function is defined as:

$$\sigma = p(x_1 - x_{1d}) \quad (3.26)$$

where $p > 0$ determines the convergence speed of the sliding motion.

Before defining the control law, it is necessary to ensure that the transversality condition

holds ($\mathcal{L}_g(\sigma) \neq 0$):

$$\mathcal{L}_g(\sigma) = \nabla\sigma \cdot g = \begin{bmatrix} p & 0 \end{bmatrix} \begin{bmatrix} 1 \\ 0 \end{bmatrix} = p \neq 0 \quad (3.27)$$

Since p is strictly positive, the transversality condition is satisfied.

The discontinuous control law is defined as:

$$u = \begin{cases} u^+ & \text{if } \sigma > 0, \\ u^- & \text{if } \sigma < 0. \end{cases} \quad (3.28)$$

where u is given by:

$$u = u_{\text{sw}} + u_{\text{eq}} = -\frac{k \text{sign}(\sigma)}{\mathcal{L}_g(\sigma)} - \frac{\mathcal{L}_f(\sigma)}{\mathcal{L}_g(\sigma)} \quad (3.29)$$

and k determines the attractiveness of the sliding surface Σ .

In this formulation:

- u_{sw} acts as a discontinuous control term that forces the trajectory onto the sliding surface.
- u_{eq} ensures that the system remains on the surface once it reaches it.

Specifically:

$$\mathcal{L}_f(\sigma) = \nabla\sigma \cdot f = p \left(a - x_1 - \frac{4 * x_1 * x_2}{1 + x_1^2} \right) \quad (3.30)$$

Substituting, the resulting control input is

$$u = -\frac{k \text{sign}(\sigma)}{p} - \left(a - x_1 - \frac{4x_1x_2}{1 + x_1^2} \right) \quad (3.31)$$

Once the sliding surface Σ is reached ($\sigma(x) = 0$), the control input reduces to $u = u_{\text{eq}}$. Consequently, the closed-loop system equation becomes:

$$\dot{x} = f(x) + g(x)u_{\text{eq}}$$

Since

$$\sigma(x) = 0 \rightarrow p(x_1 - x_{1d}) = 0 \rightarrow x_1 = x_{1d}$$

differentiating $x_1 = x_{1d}$ gives:

$$\dot{x}_1 = 0$$

Consequentially:

$$\dot{x}_2 = b x_{1d} \left(1 - \frac{x_2}{1 + x_{1d}^2} \right). \quad (3.32)$$

The dynamic for x_2 is the same obtained for the internal dynamics studied via Feedback Linearization in the previous section. Once again, since $b = 2 > 0$, it is stable. As a consequence, the closed-loop system under Sliding Mode Control is asymptotically stable. A known drawback of the discontinuous control law in (3.29) is the phenomenon of chattering, a high-frequency oscillation caused by the rapid switching of the control action. This may damage actuators or lead to undesirable oscillations. To mitigate this effect, the

sign function is replaced with a saturation function, introducing a boundary layer around the switching surface:

$$\text{sat}\left(\frac{\sigma}{\epsilon}\right) = \begin{cases} \frac{\sigma}{\epsilon} & \text{if } |\sigma| < \epsilon \\ \text{sign}\left(\frac{\sigma}{\epsilon}\right) & \text{if } |\sigma| \geq \epsilon \end{cases} \quad (3.33)$$

where ϵ defines the boundary layer thickness.

By choosing $p = 1$, $k = 3$ and $\epsilon = 0.1$ the Simulink scheme implementing the Sliding Mode Controller is shown in Fig. 3.26.

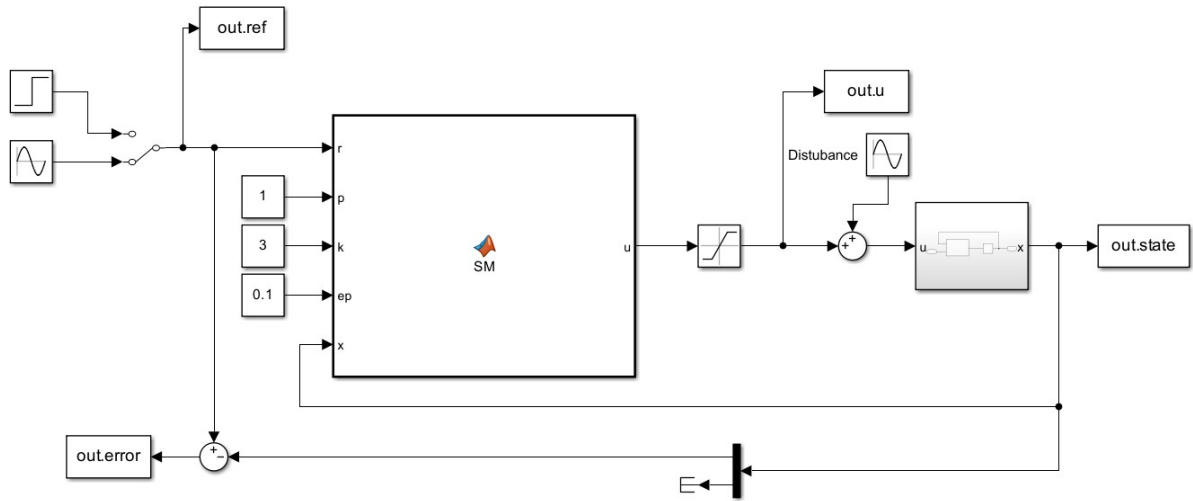


Figure 3.26: Control Scheme with the Sliding Mode Controller.

The first simulation is carried out with a constant reference. As illustrated in Fig. 3.27-3.29, the output successfully tracks the desired reference, meeting the performance specifications as follows:

- Steady-state error: $|e_\infty| = 0\%$;
- Settling time 1%: $t_{s,1\%} \approx 1$ s;
- Maximum control input: $\|u\|_\infty = 15$.

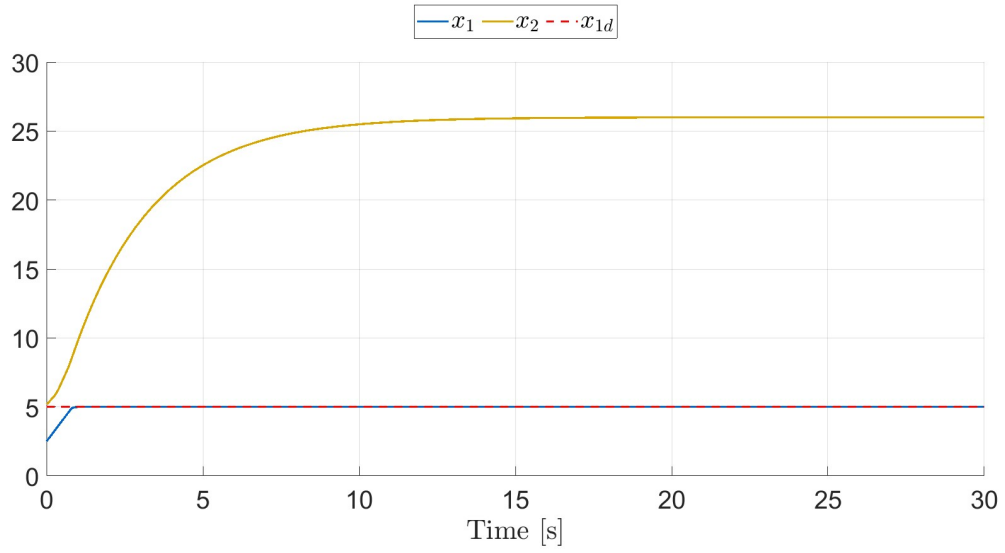


Figure 3.27: State Trajectories using SM Controller with $x_{1d} = 5$, without parametric uncertainties or disturbances.

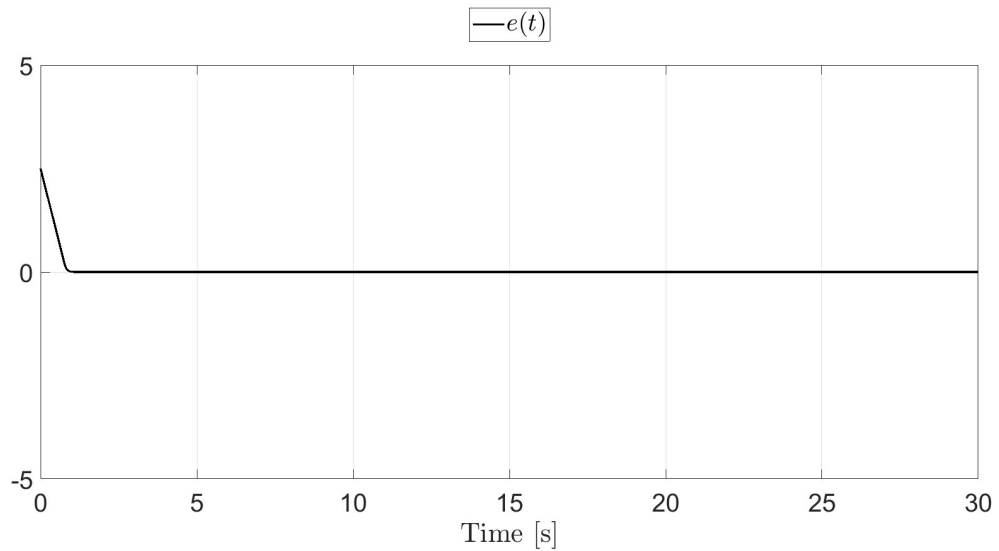


Figure 3.28: Error evolution $e = x_{1d} - x_1$ using SM Controller with $x_{1d} = 5$, without parametric uncertainties or disturbances.

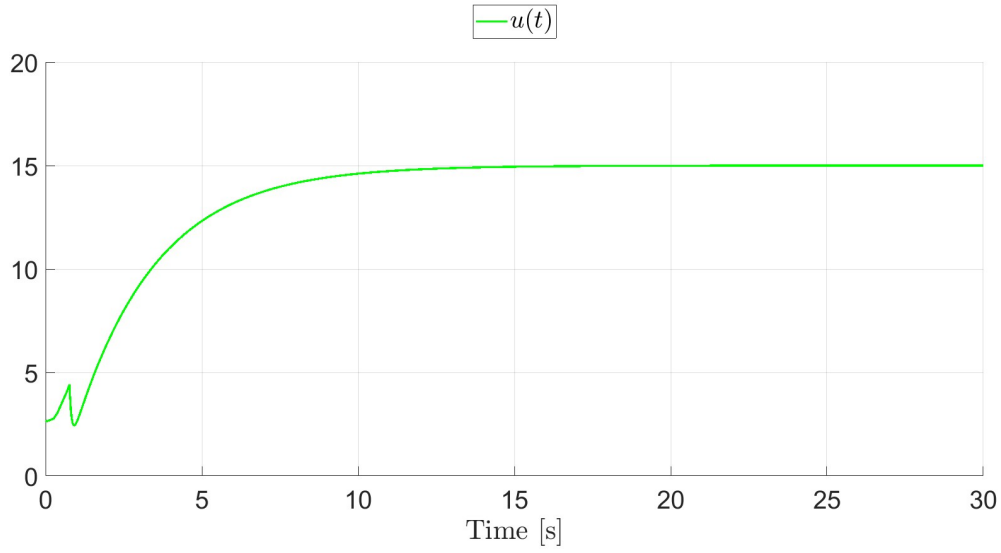


Figure 3.29: Control Input using SM Controller with $x_{1d} = 5$, without parametric uncertainties or disturbances.

The system is now tested with a sinusoidal reference input. The results shown in the following figures indicate that the SM controller effectively tracks both low and high frequency sinusoidal references, even with larger amplitudes, with minimal steady-state error and a really fast settling time. In all simulations, the steady-state error remains around $|e_\infty| = 0.03\%$, while the settling time is approximately $t_{s,1\%} \approx 1s$.

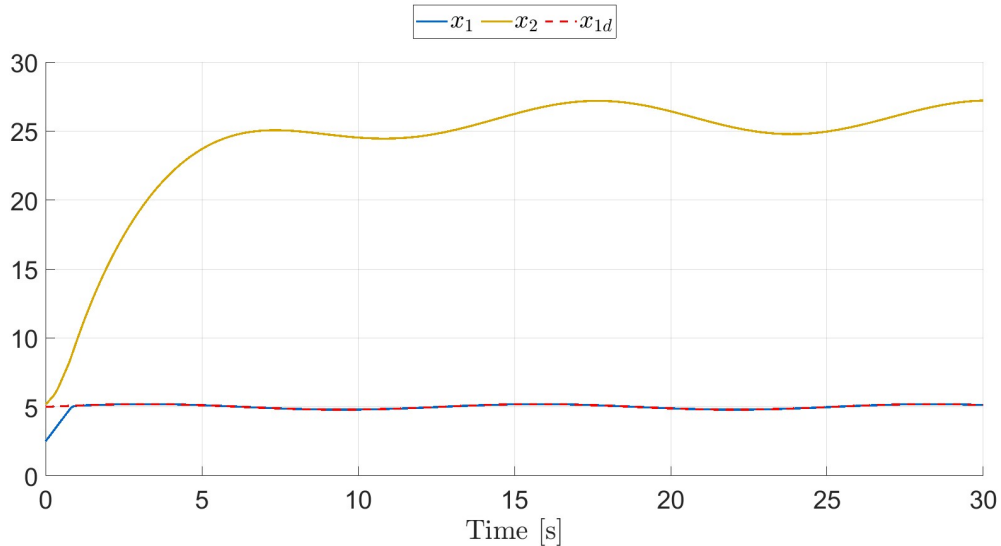


Figure 3.30: State Trajectories using SM Controller with $x_{1d} = 5 + 0.2 \sin(0.5t)$, without parametric uncertainties or disturbances.

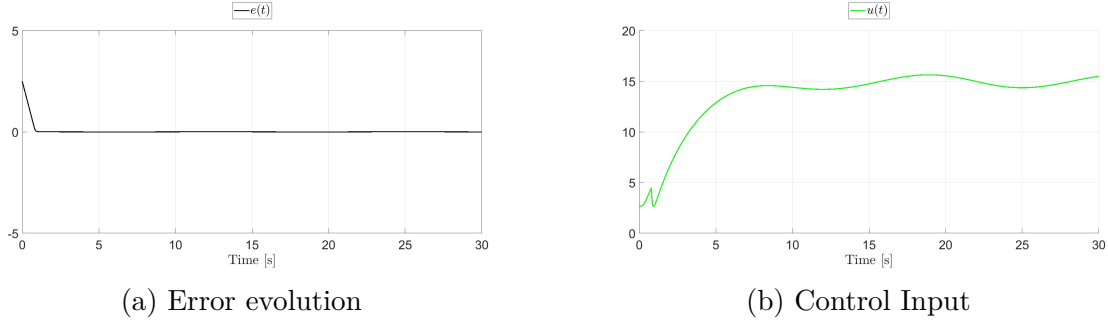


Figure 3.31: Error evolution (a) and Control Input (b) using SM Controller with $x_{1d} = 5 + 0.2 \sin(0.5t)$, without parametric uncertainties or disturbances.

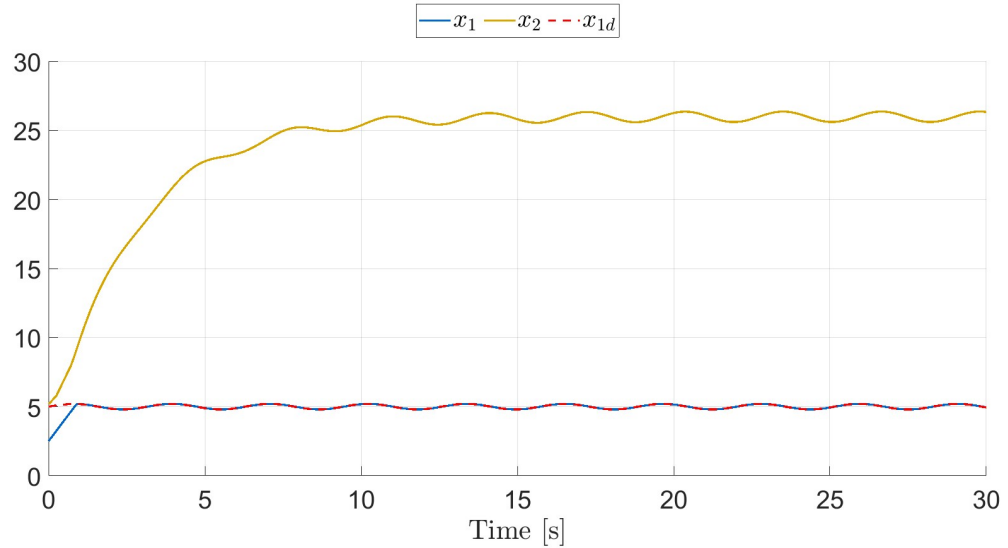


Figure 3.32: State Trajectories using SM Controller with $x_{1d} = 5 + 0.2 \sin(2t)$, without parametric uncertainties or disturbances.

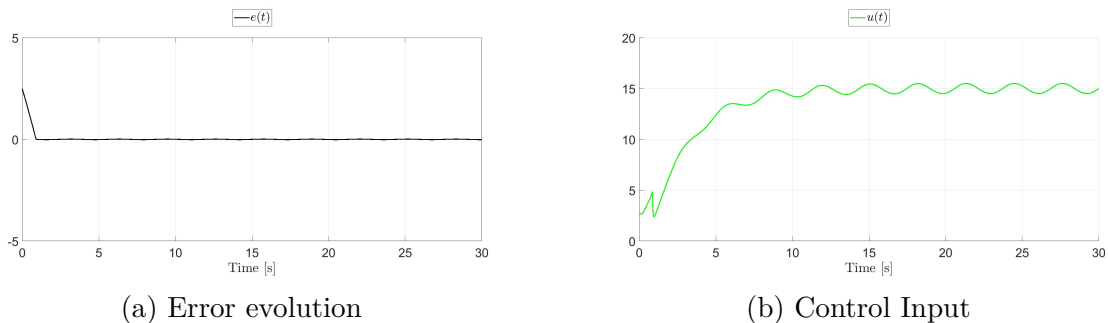


Figure 3.33: Error evolution (a) and Control Input (b) using SM Controller with $x_{1d} = 5 + 0.2 \sin(2t)$, without parametric uncertainties or disturbances.

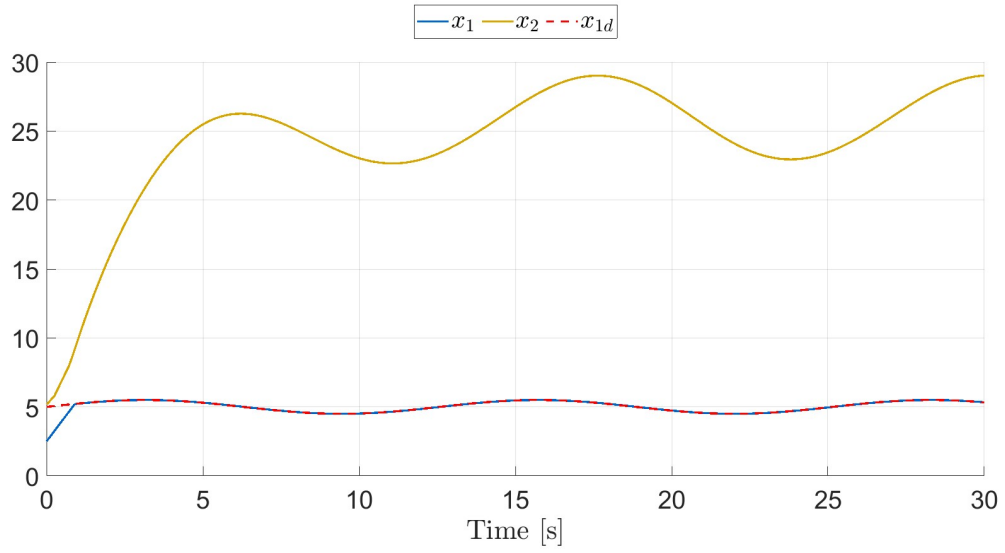


Figure 3.34: State Trajectories using SM Controller with $x_{1d} = 5 + 0.5 \sin(0.5t)$, without parametric uncertainties or disturbances.

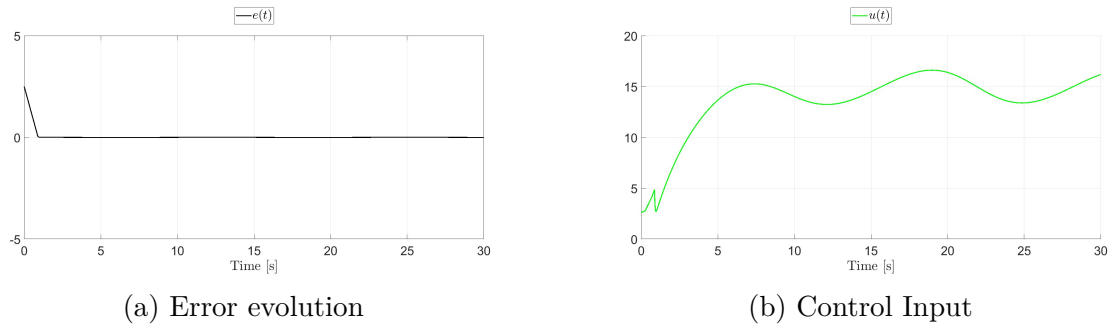


Figure 3.35: Error evolution (a) and Control Input (b) using SM Controller with $x_{1d} = 5 + 0.5 \sin(0.5t)$, without parametric uncertainties or disturbances.

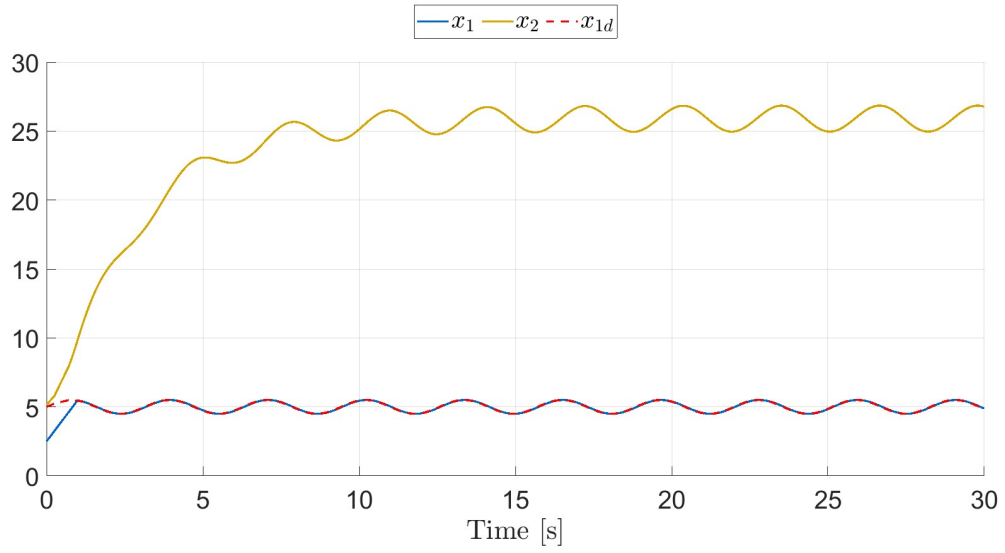


Figure 3.36: State Trajectories using SM Controller with $x_{1d} = 5 + 0.5 \sin(2t)$, without parametric uncertainties or disturbances.

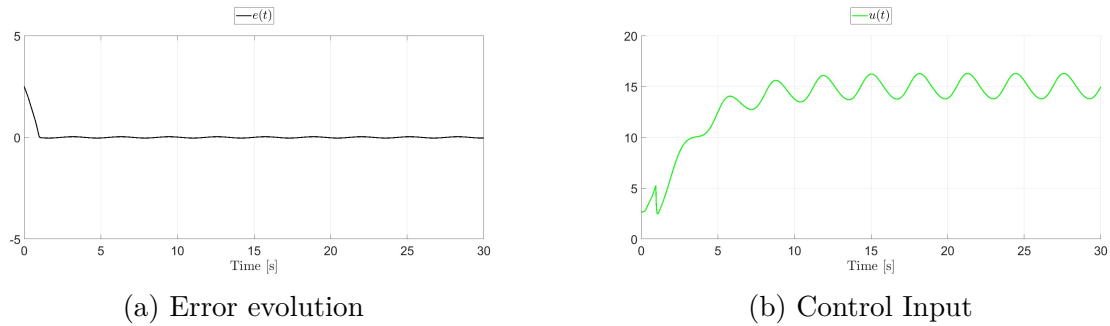


Figure 3.37: Error evolution (a) and Control Input (b) using SM Controller with $x_{1d} = 5 + 0.5 \sin(2t)$, without parametric uncertainties or disturbances.

Chapter 4

Robustness Analysis

Since the controllers analyzed in the previous chapter were tested without parametric uncertainties or disturbances, a robustness analysis is necessary to evaluate their performance. In this chapter, the controllers are tested separately under two different scenarios:

- The presence of a sinusoidal disturbance applied to the input with two different amplitudes: $d(t) = 0.3 \sin(t)$ and $d(t) = 0.6 \sin(t)$.
- Parametric uncertainties of 10% and 20% relative to their nominal values.

The robustness analysis is performed using the constant input reference $x_{1d} = 5$.

4.1 Disturbance on the Input

Firstly, the controllers are tested in the presence of a sinusoidal disturbance $d(t) = 0.3 \sin(t)$ applied to the input without parametric uncertainties.

As shown in Fig. 4.1-4.2, the LQ Controller performs well despite the disturbance. The settling time increases slightly, reaching 7.3 s, after that the error stabilizes at zero. This indicates that the LQ Controller effectively rejects the disturbance while maintaining a good transient response.

Regarding the Feedback Linearization Control, the controller does not achieve an error below the 1% threshold. However, the steady-state error $|e_\infty| = 0.07$ is still well within acceptable limits. These results are shown in Fig. 4.3-4.4.

The Sliding Mode Control demonstrates its robustness to matched disturbances, such as those applied to the input. In fact, the settling time remains comparable to the results obtained in the previous chapter in the absence of disturbances. Additionally, the steady-state performance remains unaffected. This can be observed in Fig. 4.5-4.6.

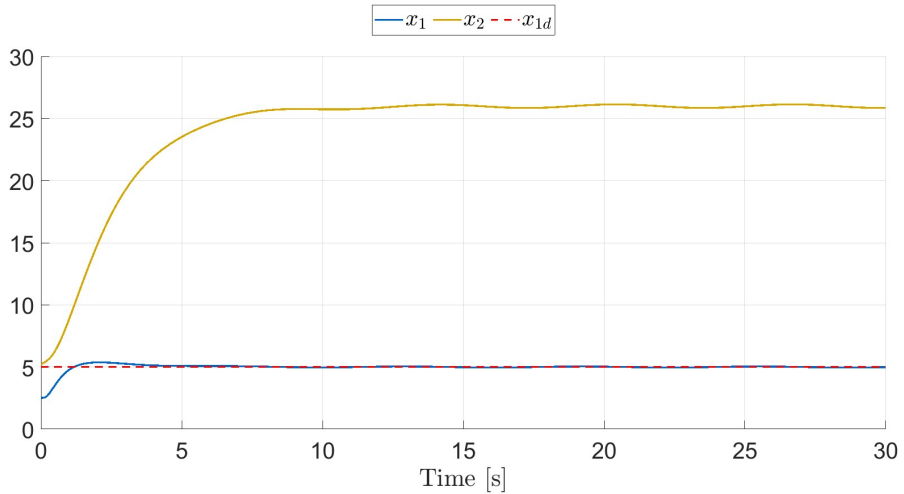


Figure 4.1: State Trajectories using LQ Controller with $x_{1d} = 5$ with a disturbance applied on the input $d(t) = 0.3 \sin(t)$.

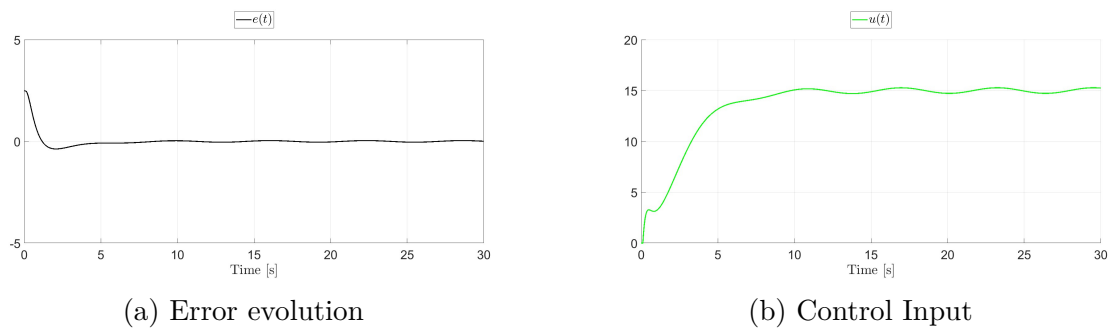


Figure 4.2: Error evolution (a) and Control Input (b) using LQ Controller with $x_{1d} = 5$ with a disturbance applied on the input $d(t) = 0.3 \sin(t)$.

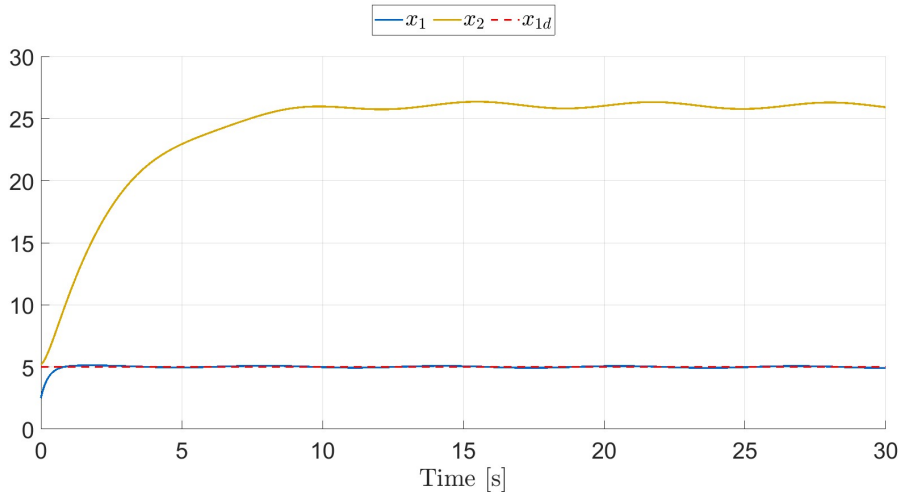


Figure 4.3: State Trajectories using FBL Controller with $x_{1d} = 5$ with a disturbance applied on the input $d(t) = 0.3 \sin(t)$.

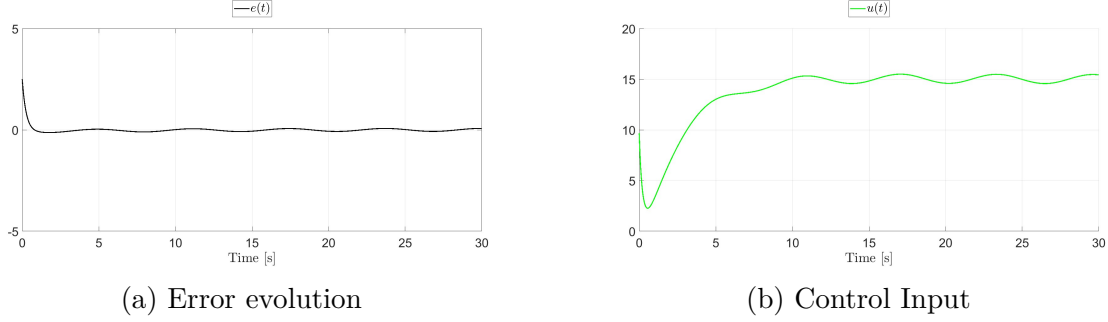


Figure 4.4: Error evolution (a) and Control Input (b) using FBL Controller with $x_{1d} = 5$ with a disturbance applied on the input $d(t) = 0.3 \sin(t)$.

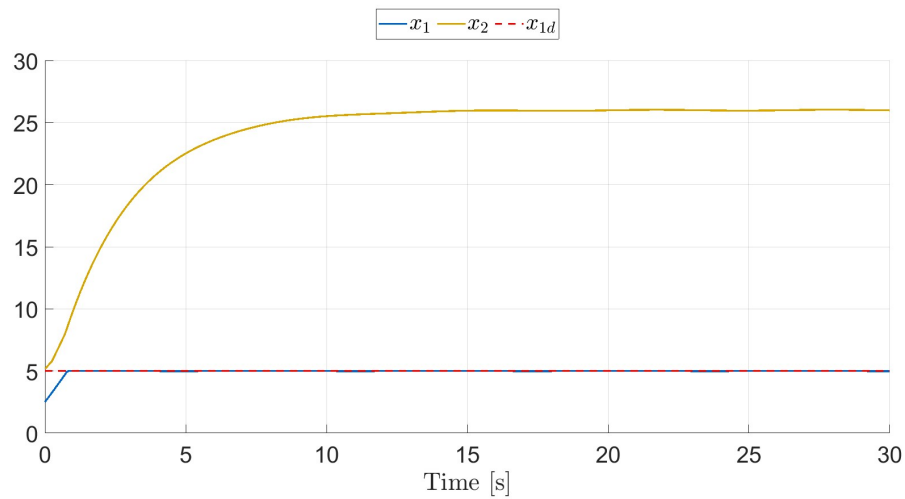


Figure 4.5: State Trajectories using SM Controller with $x_{1d} = 5$ with a disturbance applied on the input $d(t) = 0.3 \sin(t)$.

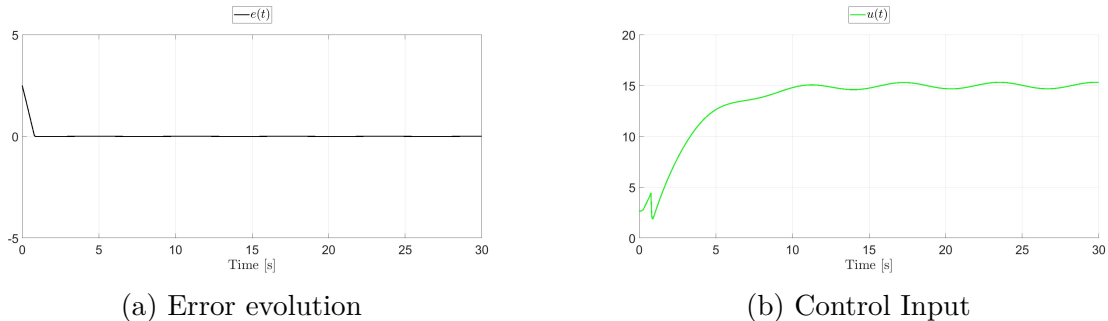


Figure 4.6: Error evolution (a) and Control Input (b) using SM Controller with $x_{1d} = 5$ with a disturbance applied on the input $d(t) = 0.3 \sin(t)$.

Increasing the amplitude of the disturbance on the input to $d(t) = 0.6 \sin(t)$, similar results can be observed in the following figures.

Specifically, the LQ Controller exhibits a significant increase in the settling time, reaching 29.4 s. However, the steady-state error remains negligible at $|e_\infty| = 0.01$, indicating that

despite a longer transient phase, the controller effectively mitigates the disturbance in steady state.

For the Feedback Linearization Controller, the system still does not meet the 1% settling time criterion, but the steady-state error rises slightly to $|e_\infty| = 0.14$.

The Sliding Mode Controller continues to demonstrate strong robustness against input disturbances even with higher amplitudes. The settling time remains nearly unchanged at 0.76 s, and the steady-state error remains small at $|e_\infty| = 0.02$.

The LQ Controller and Feedback Linearization Controller exhibit a smoother control input compared to the SM Controller.

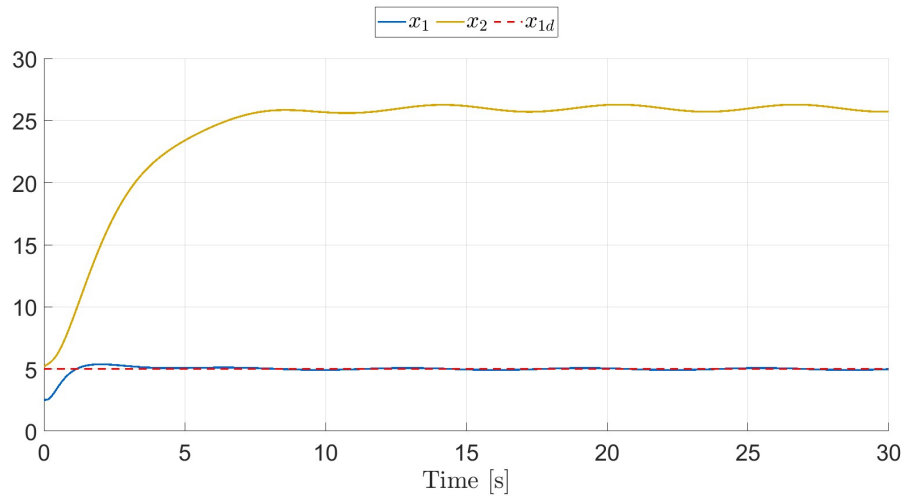


Figure 4.7: State Trajectories using LQ Controller with $x_{1d} = 5$ with a disturbance applied on the input $d(t) = 0.6 \sin(t)$.

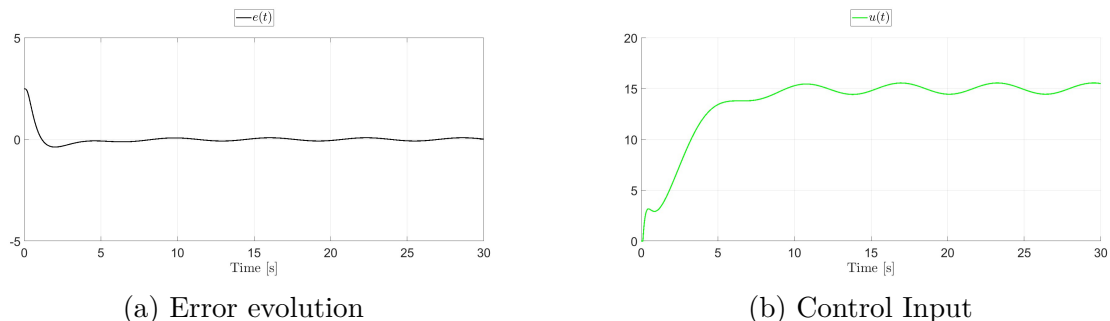


Figure 4.8: Error evolution (a) and Control Input (b) using LQ Controller with $x_{1d} = 5$ with a disturbance applied on the input $d(t) = 0.6 \sin(t)$.

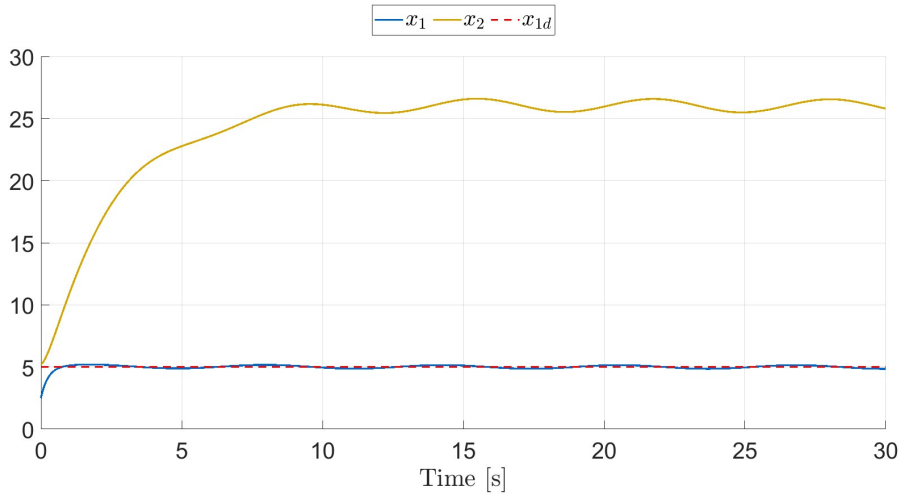


Figure 4.9: State Trajectories using FBL Controller with $x_{1d} = 5$ with a disturbance applied on the input $d(t) = 0.6 \sin(t)$.

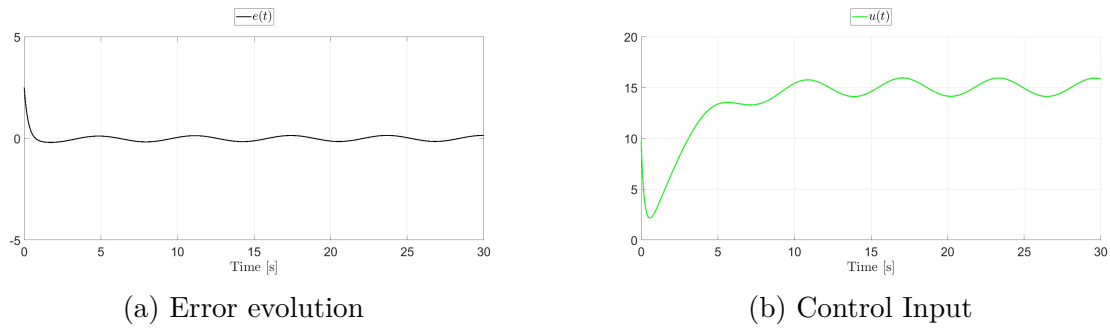


Figure 4.10: Error evolution (a) and Control Input (b) using FBL Controller with $x_{1d} = 5$ with a disturbance applied on the input $d(t) = 0.6 \sin(t)$.

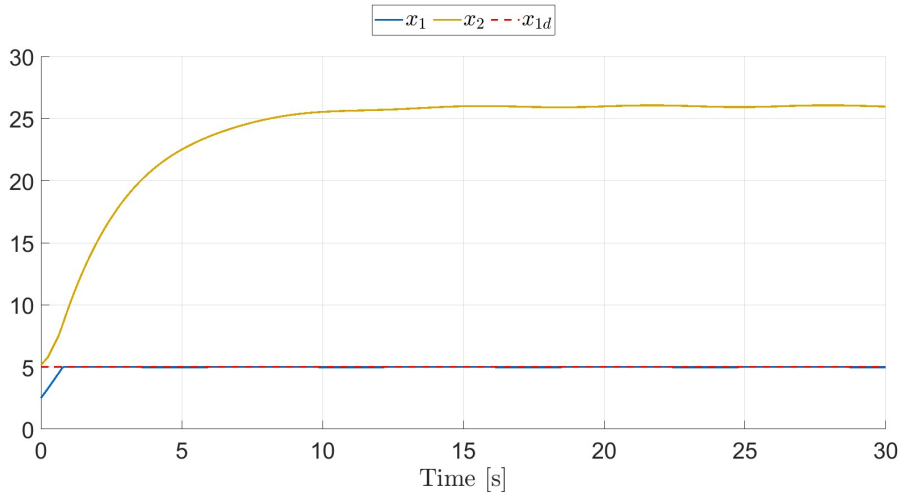


Figure 4.11: State Trajectories using SM Controller with $x_{1d} = 5$ with a disturbance applied on the input $d(t) = 0.6 \sin(t)$.

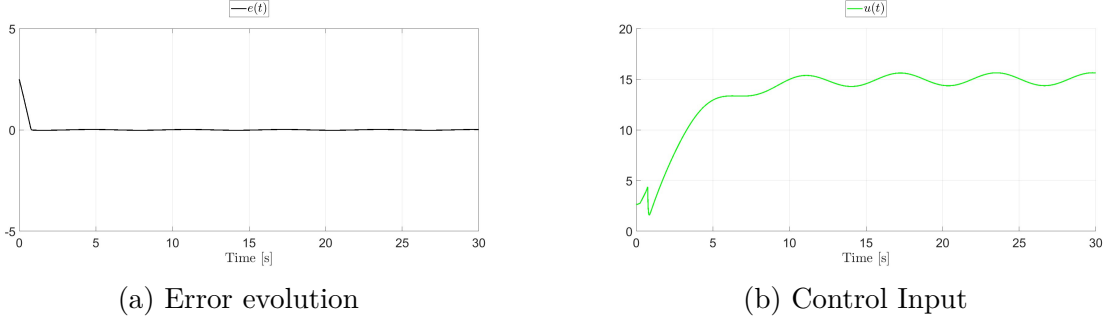


Figure 4.12: Error evolution (a) and Control Input (b) using SM Controller with $x_{1d} = 5$ with a disturbance applied on the input $d(t) = 0.6 \sin(t)$.

4.2 Parametric Uncertainties

The controllers are tested under parametric uncertainties without input disturbances. Firstly, a 10% uncertainty with respect to the nominal values (\bar{a}, \bar{b}) is introduced, specifically:

$$a = 0.9\bar{a}, \quad b = 1.1\bar{b}$$

The LQ Controller maintains good tracking performance, achieving a settling time of 5.52 s. Despite this, the steady-state error remains zero, confirming that the controller can handle small parametric variations effectively.

The Feedback Linearization Controller shows a more conservative response with a longer settling time of 9.74s. However, the steady-state error remains at zero.

The Sliding Mode Controller continues to demonstrate strong robustness even against parametric uncertainties. The settling time increases slightly to 1.23 s, but remains significantly lower than the other controllers. The steady-state error is slightly higher at $|e_\infty| = 0.03$ compared to the nominal case.

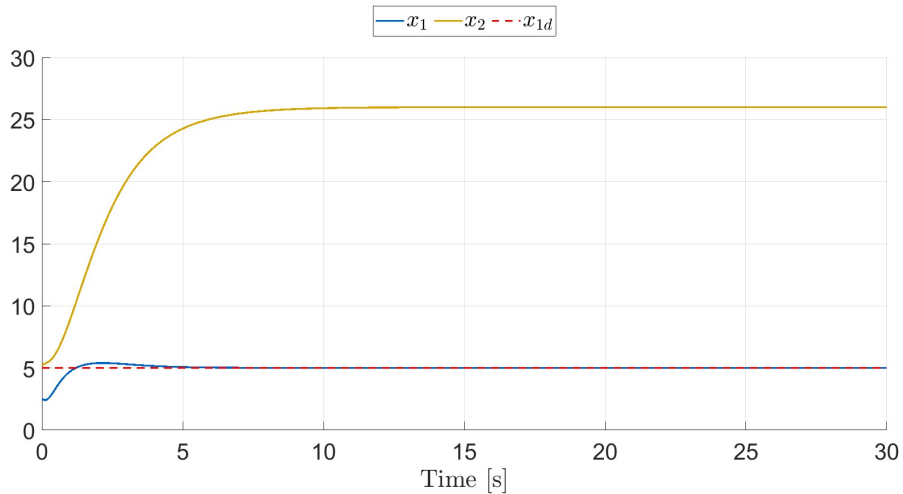


Figure 4.13: State Trajectories using LQ Controller with $x_{1d} = 5$ with parametric uncertainties of 10% relative to their nominal values.

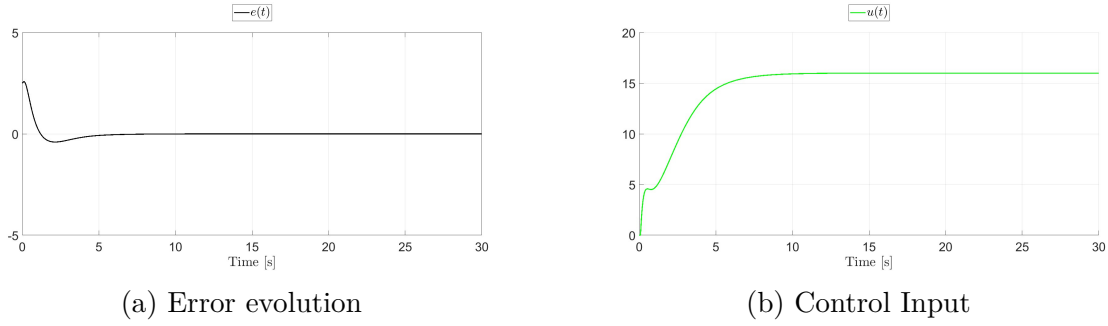


Figure 4.14: Error evolution (a) and Control Input (b) using LQ Controller with parametric uncertainties of 10% relative to their nominal values.

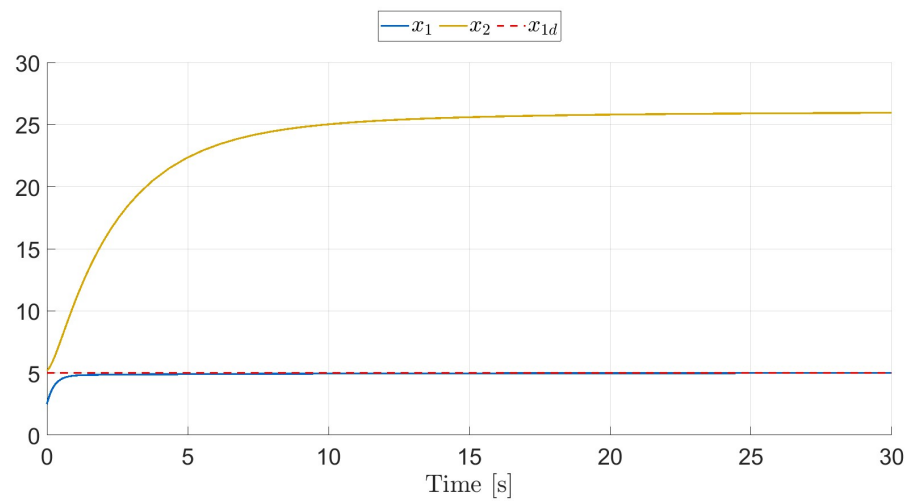


Figure 4.15: State Trajectories using FBL Controller with $x_{1d} = 5$ with parametric uncertainties of 10% relative to their nominal values.

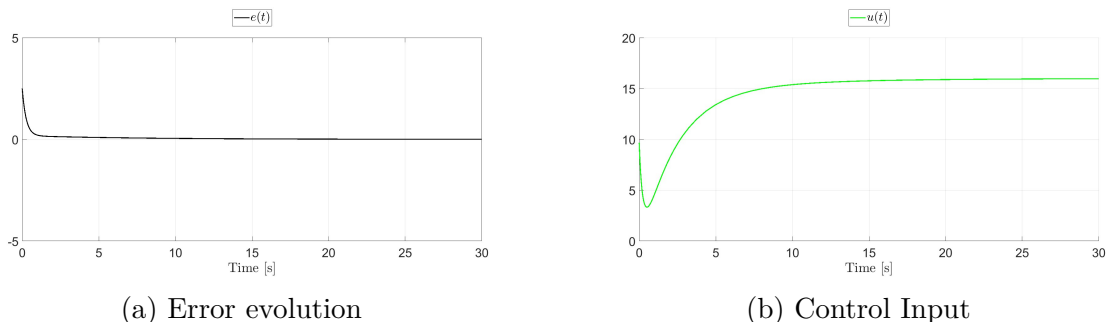


Figure 4.16: Error evolution (a) and Control Input (b) using FBL Controller with parametric uncertainties of 10% relative to their nominal values.

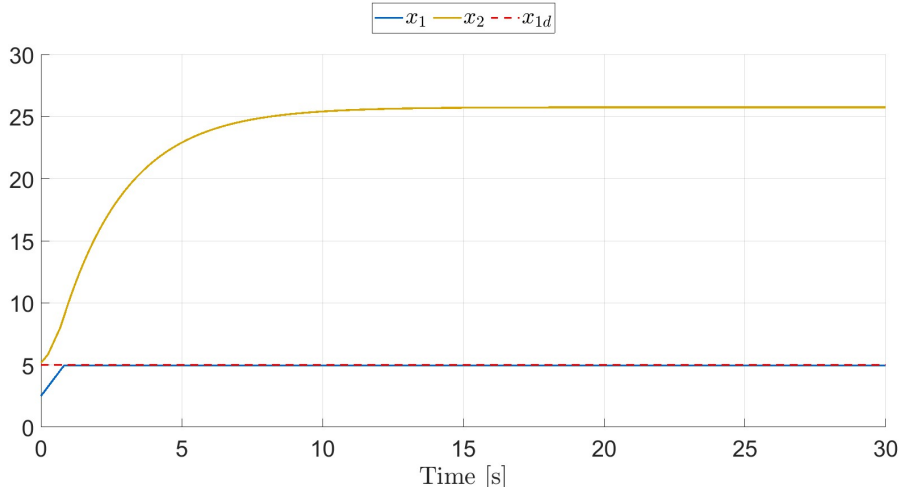


Figure 4.17: State Trajectories using SM Controller with $x_{1d} = 5$ with parametric uncertainties of 10% relative to their nominal values.

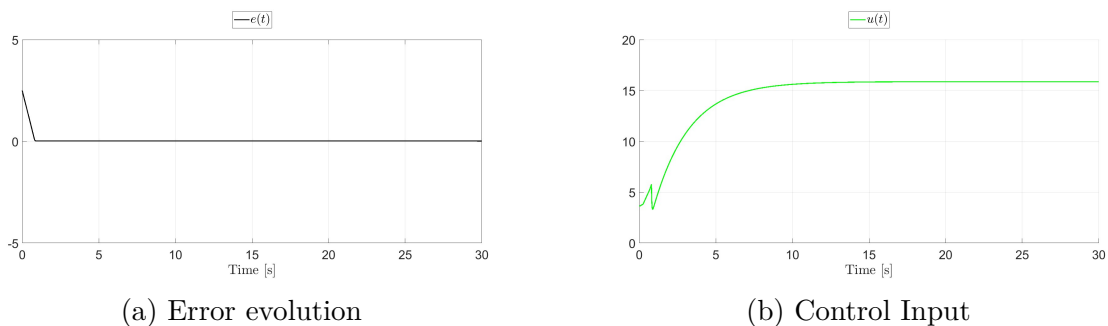


Figure 4.18: Error evolution (a) and Control Input (b) using SM Controller with parametric uncertainties of 10% relative to their nominal values.

A second simulation is performed considering a 20% uncertainties with respect to the nominal values (\bar{a}, \bar{b}) , specifically:

$$a = 1.2\bar{a}, \quad b = 0.8\bar{b}$$

The LQ Controller shows an increase in settling time to 6.72 s, while maintaining zero steady-state error. The overshoot is slightly reduced compared to the 10% uncertainty case, reaching 6.03%. The control input remains within acceptable bounds.

The Feedback Linearization Controller exhibits a significant increase in settling time, reaching 19.47 s, with a higher overshoot. The steady-state error remains minimal at $|e_\infty| = 0.01$.

For the Sliding Mode Controller, the effect of the increased parametric uncertainty is more noticeable. The control input saturates at 0. Despite the settling time requirement is not met, the steady-state error remains small at $|e_\infty| = 0.06$. This suggests that performance could be improved by increasing the gain k , allowing the controller to be more robust.

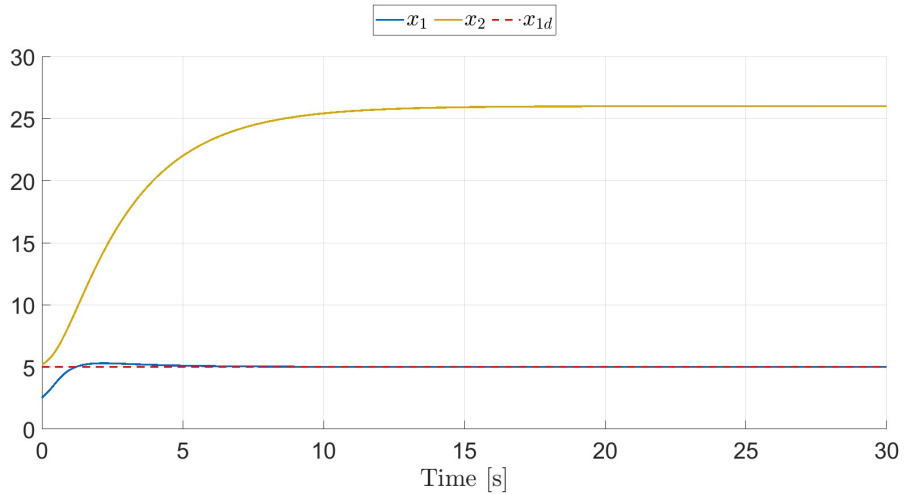


Figure 4.19: State Trajectories using LQ Controller with $x_{1d} = 5$ with parametric uncertainties of 20% relative to their nominal values.

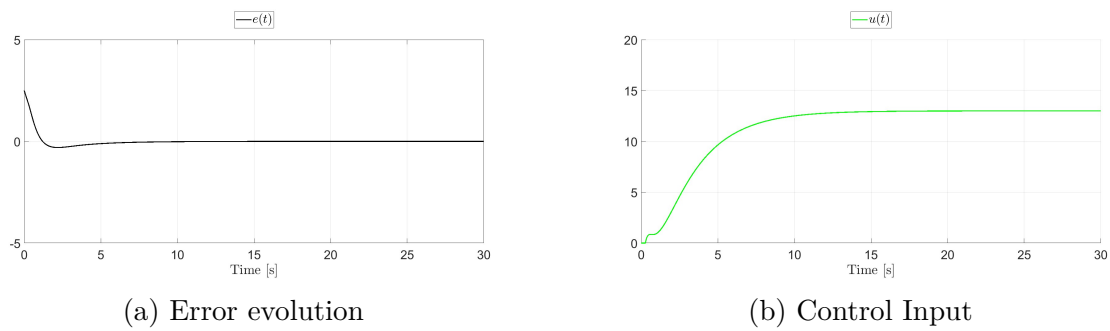


Figure 4.20: Error evolution (a) and Control Input (b) using LQ Controller with parametric uncertainties of 20% relative to their nominal values.

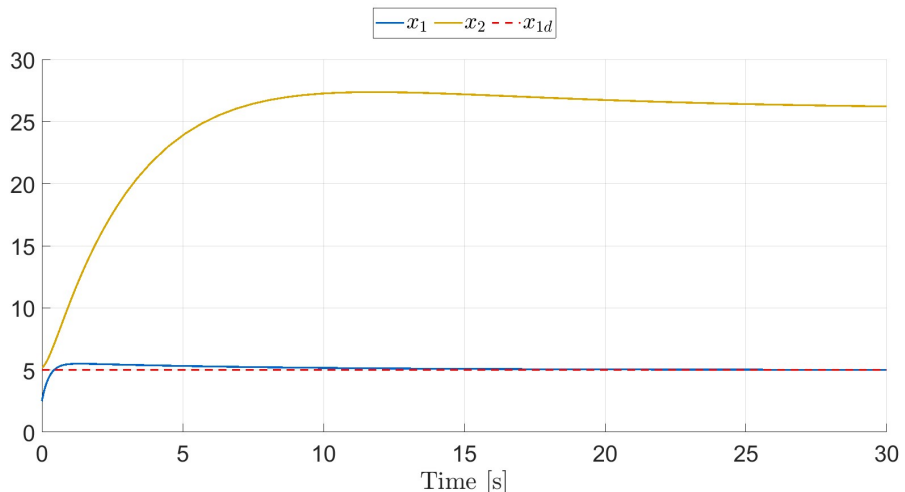


Figure 4.21: State Trajectories using FBL Controller with $x_{1d} = 5$ with parametric uncertainties of 20% relative to their nominal values.

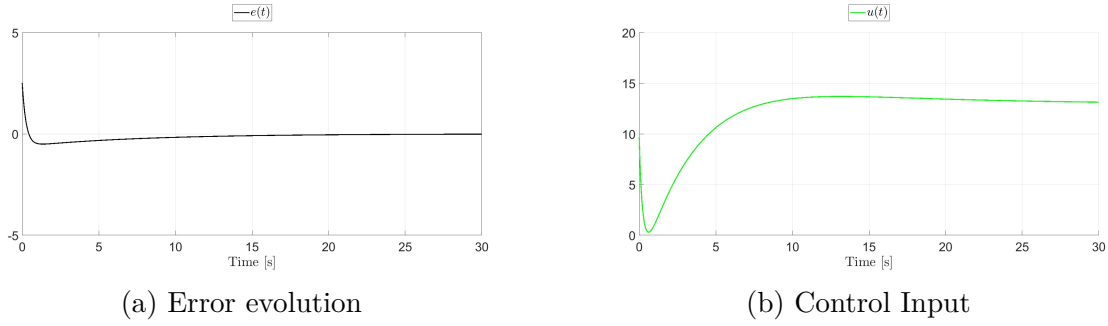


Figure 4.22: Error evolution (a) and Control Input (b) using FBL Controller with parametric uncertainties of 20% relative to their nominal values.

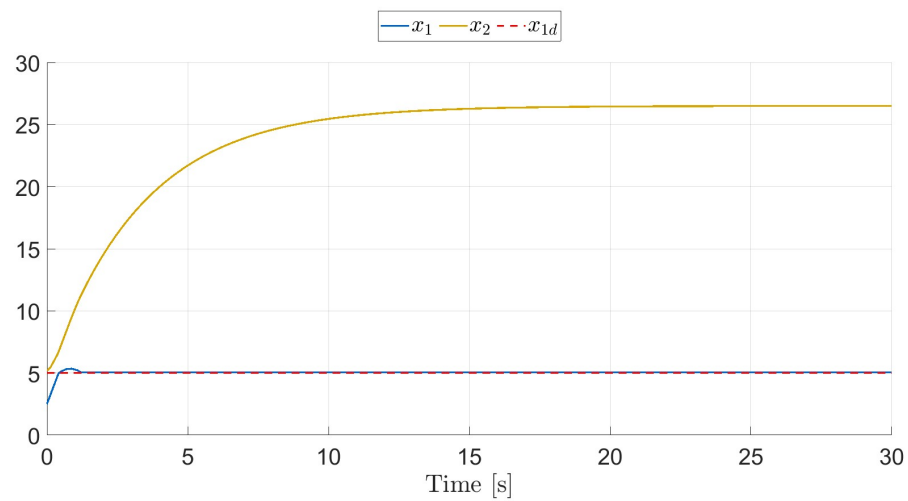


Figure 4.23: State Trajectories using SM Controller with $x_{1d} = 5$ with parametric uncertainties of 20% relative to their nominal values.

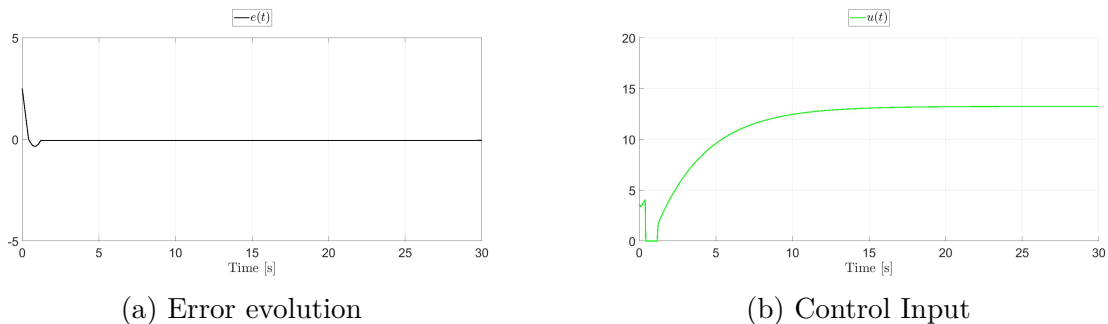


Figure 4.24: Error evolution (a) and Control Input (b) using SM Controller with parametric uncertainties of 20% relative to their nominal values.

Chapter 5

Conclusion and Controllers Comparison

In this project, the CIMA reaction was analyzed and controlled.

Firstly, **Chapter 1** presented the derivation of the two-variable nonlinear model from the chlorine dioxide–iodine–malonic acid reaction and its empirical rate laws, highlighting the key parameters of the system.

Then, **Chapter 2** explored the open-loop behavior of the system, analyzing its stability properties. By varying the parameter b , the presence of a Hopf bifurcation was identified. Subsequently, in **Chapter 3**, three different control techniques were implemented to regulate and analyze the concentration of iodide, ensuring that the desired specifications were met. These techniques are the LQ Optimal Controller, designed using the linearized model around the equilibrium point, the I/O Feedback Linearization Controller and the Sliding Mode Controller.

Finally, in **Chapter 4**, a robustness analysis was conducted to evaluate the controllers' performance in presence of input disturbances and parametric uncertainties.

The results obtained in **Chapter 3** and **Chapter 4** are summarized in the following tables to make controllers' comparison.

As far as the constant input without disturbances and without parametric uncertainties is concerned, the three controllers perform very well as shown in Table 5.1. The SM controller presents a faster settling time with respect the other two controller. All of them presents 0 steady state error. The LQ controller shows a higher overshoot. The maximum value of the control input of all the controllers is comparable.

Controller	$t_{s,1\%}$ [s]	PO [%]	$ e_\infty $	$\ u\ _\infty$
LQ	5.08	7.39	0.00	15
FBL	3.92	1.32	0.00	15.05
SM	0.81	0.00	0.00	14.99

Table 5.1: Performance comparison of LQ, FBL and SM Controllers with $x_{1d} = 5$ without parametric uncertainties or disturbances.

Regarding the sinusoidal reference, for simplicity, only the results for $x_{1d} = 5 + 0.2 \sin(0.5t)$ and $x_{1d} = 5 + 0.5 \sin(2t)$ are reported respectively in Tables 5.2 and 5.3.

The results show that the LQ Controller is able to track the desired sinusoidal signal when

the frequency and amplitude are low, although the settling time and overshoot increase. However, when the signal has both high amplitude and high frequency, the controller struggles to follow the reference, resulting in a high steady-state error.

On the other hand, the Feedback Linearization Controller and Sliding Mode Controller effectively track the desired sinusoidal signals in both cases, meeting the desired performance specifications.

Controller	$t_{s,1\%}$ [s]	PO [%]	$ e_\infty $	$\ u\ _\infty$
LQ	6.28	8.14	0.04	15.78
FBL	4.00	2.50	0.00	15.70
SM	0.84	1.36	0.00	15.63

Table 5.2: Performance comparison of LQ, FBL and SM Controllers with $x_{1d} = 5 + 0.2 \sin(0.5t)$ without parametric uncertainties or disturbances.

Controller	$t_{s,1\%}$ [s]	PO [%]	$ e_\infty $	$\ u\ _\infty$
LQ	-	17	0.6	17.00
FBL	4.73	14.62	0.00	16.35
SM	0.97	13.44	0.03	16.29

Table 5.3: Performance comparison of LQ, FBL and SM Controllers with $x_{1d} = 5 + 0.5 \sin(2t)$ without parametric uncertainties or disturbances.

Concerning the robustness analysis, Tables 5.4 and 5.5 present respectively the results for input disturbances of $d(t) = 0.3 \sin(t)$ and $d(t) = 0.6 \sin(t)$, while Tables 5.6 and 5.7 report respectively the results for parametric uncertainties of 10% and 20% relative to the nominal values.

Specifically, the LQ Controller effectively tracks the reference in presence of input disturbances, but at the cost of a longer settling time and higher overshoot compared to the SM Controller. Conversely, with parametric uncertainties, it achieves better performance in a shorter time.

On the other hand, the FBL Controller with input disturbances fails to meet the 1% settling time requirement, although the steady-state error remains small, ranging between 0.07 and 0.14. Regarding parametric uncertainties, the FBL controller performs well with small variations in parameters but exhibits a longer response time and larger overshoot as the amplitude of the uncertainties increases.

Finally, the SM Controller demonstrates the best robustness, achieving satisfactory results in both input disturbance and parametric uncertainty scenarios. It consistently provides fast response, low overshoot, and minimal steady-state error.

Controller	$t_{s,1\%}$ [s]	PO [%]	$ e_\infty $	$\ u\ _\infty$
LQ	7.3	7.44	0.00	15.27
FBL	-	2.64	0.07	15.50
SM	0.78	0.20	0.00	15.31

Table 5.4: Performance comparison of LQ, FBL and SM Controllers with $x_{1d} = 5$ with a disturbance applied on the input $d(t) = 0.3 \sin(t)$.

Controller	$t_{s,1\%}$ [s]	PO [%]	$ e_\infty $	$\ u\ _\infty$
LQ	29.4	7.53	0.01	15.55
FBL	-	3.97	0.14	15.94
SM	0.76	0.40	0.02	15.63

Table 5.5: Performance comparison of LQ, FBL and SM Controllers with $x_{1d} = 5$ with a disturbance applied on the input $d(t) = 0.6 \sin(t)$.

Controller	$t_{s,1\%}$ [s]	PO [%]	$ e_\infty $	$\ u\ _\infty$
LQ	5.52	8.05	0.00	16.00
FBL	9.74	0.00	0.00	15.96
SM	1.23	0.00	0.03	15.83

Table 5.6: Performance comparison of LQ, FBL and SM Controllers with $x_{1d} = 5$ with parametric uncertainties of 10%.

Controller	$t_{s,1\%}$ [s]	PO [%]	$ e_\infty $	$\ u\ _\infty$
LQ	6.72	6.03	0.00	12.99
FBL	19.47	10.09	0.01	13.69
SM	-	5.37	0.06	13.33

Table 5.7: Performance comparison of LQ, FBL and SM Controllers with $x_{1d} = 5$ with parametric uncertainties of 20%.

Bibliography

- [1] Strogatz, S. H. (2015). *Nonlinear Dynamics and Chaos: With Applications to Physics, Biology, Chemistry, and Engineering* (2nd ed.). CRC Press. <https://doi.org/10.1201/9780429492563>
- [2] Lengyel, I., Rabai, G. and Epstein, I. R. (1990). Experimental and modeling study of oscillations in the chlorine dioxide-iodine-malonic acid reaction. *Journal of the American Chemical Society*, 112, 9104.
- [3] Din, Q., Donchev, T., Kolev, D. (2018). Stability, bifurcation analysis and chaos control in chlorine dioxide–iodine–malonic acid reaction. *MATCH Communications in Mathematical and in Computer Chemistry*, 79(3), 577–606.
- [4] Shapiro, J. E. *Dfield and Pplane: Java Tools for Phase Plane Analysis*. Available at: <https://www.cs.unm.edu/~joel/dfield/>.
- [5] MatCont Development Team. *MatCont: A MATLAB package for numerical bifurcation analysis*. Available at: <https://sourceforge.net/projects/matcont/>.
- [6] MathWorks. *Linear-Quadratic Regulator (LQR) design*. Available at: <https://www.mathworks.com/help/control/ref/lti.lqr.html>.